

Improving the Model Consistency of Decentralized Federated Learning

Yifan Shi¹ Li Shen² Kang Wei³ Yan Sun² Bo Yuan¹ Xueqian Wang¹ Dacheng Tao²

Abstract

To mitigate the privacy leakages and communication burdens of Federated Learning (FL), decentralized FL (DFL) discards the central server and each client only communicates with its neighbors in a decentralized communication network. However, existing DFL suffers from high inconsistency among local clients, which results in severe distribution shift and inferior performance compared with centralized FL (CFL), especially on heterogeneous data or sparse communication topology. To alleviate this issue, we propose two DFL algorithms named DFedSAM and DFedSAM-MGS to improve the performance of DFL. Specifically, DFedSAM leverages gradient perturbation to generate local flat models via Sharpness Aware Minimization (SAM), which searches for models with uniformly low loss values. DFedSAM-MGS further boosts DFedSAM by adopting Multiple Gossip Steps (MGS) for better model consistency, which accelerates the aggregation of local flat models and better balances communication complexity and generalization. Theoretically, we present improved convergence rates $\mathcal{O}(\frac{1}{\sqrt{KT}} + \frac{1}{T} + \frac{1}{K^{1/2}T^{3/2}(1-\lambda)^2})$ and $\mathcal{O}(\frac{1}{\sqrt{KT}} + \frac{1}{T} + \frac{\lambda^Q+1}{K^{1/2}T^{3/2}(1-\lambda^Q)^2})$ in non-convex setting for DFedSAM and DFedSAM-MGS, respectively, where $1 - \lambda$ is the spectral gap of gossip matrix and Q is the number of MGS. Empirically, our methods can achieve competitive performance compared with CFL methods and outperform existing DFL methods.

1. Introduction

Federated learning (FL) (McMahan et al., 2017; Li et al., 2020b) allows distributed clients to collaboratively train a

¹Tsinghua University, Shenzhen, China ²JD Explore Academy, Beijing, China ³Nanjing University of Science and Technology, Nanjing, China. Correspondence to: Xueqian Wang <wang.xq@sz.tsinghua.edu.cn>, Li Shen <mathshenli@gmail.com>.

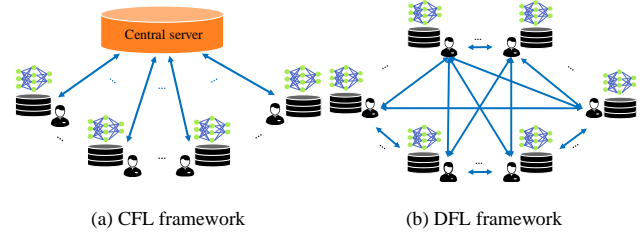


Figure 1. Illustrations of CFL (a) and DFL (b). For DFL, the various communication topologies are illustrated in **Appendix A**.

shared model under the orchestration of the cloud without transmitting local data. However, almost all FL paradigms employ a central server to communicate with clients, which faces several critical challenges, such as computational resources limitation, high communication bandwidth cost, and privacy leakage (Kairouz et al., 2021). Compared to the centralized FL (CFL, Figure 1(a)), decentralized FL (DFL, Figure 1(b)), where the clients only communicate with their neighbors without a central server, offers communication advantage and further preserves the data privacy (Kairouz et al., 2021; Wang et al., 2021; Sun et al., 2022).

However, DFL suffers from severe inconsistency among local models due to heterogeneous data distribution and model aggregation locality caused by the intrinsic network connectivity. This inconsistency may result in severe over-fitting in local models and performance degradation (Sun et al., 2022). To explore the mechanism behind this phenomenon, we present the structure of the loss landscapes (Li et al., 2018) for FedAvg (McMahan et al., 2017) and decentralized FedAvg (DFedAvg, Sun et al. (2022)) on Fashion-MNIST (Xiao et al., 2017) with the same setting in Figure 2. It is clear that DFL has a sharper landscape than CFL.

Motivation. Most FL algorithms face the over-fitting issue of local models on heterogeneous data. Many efforts (Sahu et al., 2018; Li et al., 2020c; Karimireddy et al., 2020; Yang et al., 2021; Acar et al., 2021; Wang et al., 2022) have been devoted to CFL with various effective solutions. In DFL, this issue is further exacerbated due to sharp loss landscape caused by the inconsistency of local models (see Figure 2). Therefore, the performance of decentralized schemes is generally worse than that of centralized schemes with the same setting (Sun et al., 2022). Consequently, an important

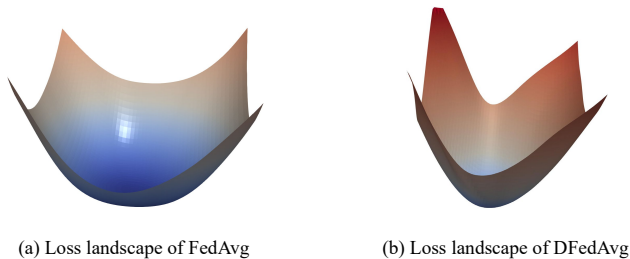


Figure 2. Loss landscapes comparison between CFL and DFL on Fashion-MNIST (Xiao et al., 2017). DFedAvg features a sharper landscape than FedAvg with poorer generalization ability.

question is: *can we design DFL algorithms that can mitigate the inconsistency among local models and achieve similar performance to its centralized counterpart?*

To answer this question, we propose two DFL algorithms: DFedSAM and DFedSAM-MGS. Specifically, DFedSAM overcomes the local over-fitting issue via gradient perturbation with SAM (Foret et al., 2021) in each client to generate local flat models. Since each client aggregates the flat models from its neighbors, a potential flat aggregated model can be generated, which results in high generalization ability. To further boost the performance of DFedSAM, DFedSAM-MGS integrates multiple gossip steps (MGS) (Ye et al., 2020; Ye & Zhang, 2021; Li et al., 2020a) to accelerate the aggregation of local flatness models by increasing the number of gossip steps of local communications. It achieves a better trade-off between communication complexity and learning performance by bridging the gap between CFL and DFL, since DFL can be roughly regarded as CFL with a sufficient number of gossip steps (Section 5.4).

Theoretically, we present the convergence rates for our algorithms in the stochastic non-convex setting. We show that the bound can be looser when the connectivity of the communication topology λ is sufficiently sparse, or the data homogeneity β is sufficiently large. Meanwhile, as the consensus/gossip steps Q in MGS increase, it is tighter as the impact of communication topology can be alleviated (Section 4). The theoretical results explain why the application of SAM and MGS in DFL can ensure better performance with various types of communication network topology. Empirically, we conduct extensive experiments on CIFAR-10 and CIFAR-100 datasets in both identical data distribution (IID) and non-IID settings. The experimental results confirm that our algorithms can achieve competitive performance compared to CFL baselines and outperform existing DFL baselines (Section 5.2).

Contribution. Our main contributions are summarized as:

- We propose two effective DFL schemes: DFedSAM and DFedSAM-MGS. DFedSAM reduces the inconsistency of local models with local flat models, and

DFedSAM-MGS further improves the consistency via MGS acceleration and features a better trade-off between communication and generalization.

- We present improved convergence rates $\mathcal{O}(\frac{1}{\sqrt{KT}} + \frac{1}{T} + \frac{1}{K^{1/2}T^{3/2}(1-\lambda)^2})$ and $\mathcal{O}(\frac{1}{\sqrt{KT}} + \frac{1}{T} + \frac{\lambda^Q+1}{K^{1/2}T^{3/2}(1-\lambda^Q)^2})$ for DFedSAM and DFedSAM-MGS in the non-convex settings, respectively, which theoretically verify the effectiveness of our approaches.
- We conduct extensive experiments to demonstrate the efficacy of DFedSAM and DFedSAM-MGS, which can achieve competitive performance compared with both CFL and DFL baselines.

2. Related Work

Decentralized Federated Learning (DFL). In DFL, clients only communicate with their neighbors in various communication networks without a central server, which offers communication advantage and better preserves data privacy in comparison to CFL. Lalitha et al. (2018; 2019) take a Bayesian-like approach to introduce a belief over the model parameter space of the clients in a fully DFL framework. Roy et al. (2019) propose the first server-less, peer-to-peer FL approach BrainTorrent and apply it to medical applications in a highly dynamic peer-to-peer FL environment. Sun et al. (2022) apply the multiple local iterations with SGD and quantization method to reduce the communication cost and provide the convergence results in various convex settings. Dai et al. (2022) develop a decentralized sparse training technique to further lower the communication and computation cost.

Sharpness Aware Minimization (SAM). SAM (Foret et al., 2021) is an effective optimizer for training deep learning models, which leverages the flat geometry of the loss landscape to improve model generalization ability. Recently, Andriushchenko & Flammarion (2022) study the properties of SAM and provide convergence results of SAM for non-convex objectives. As an effective optimizer, SAM and its variants have been applied to various machine learning (ML) tasks (Zhao et al., 2022; Kwon et al., 2021; Du et al., 2021; Liu et al., 2022; Abbas et al., 2022). For instance, Qu et al. (2022) and Caldarola et al. (2022) adopt SAM to improve generalization, and thus mitigate the distribution shift problem and achieve SOTA performance for CFL. However, to the best of our knowledge, few if any efforts have been devoted to the empirical performance and theoretical analysis of SAM in the DFL setting.

Multiple Gossip Steps (MGS). The advantage of increasing the frequency of local communications within a network topology is investigated in FastMix (Ye et al.,

2020), in which the optimal computational complexity and near-optimal communication complexity are established. DeEPCA (Ye & Zhang, 2021) integrates FastMix into a decentralized PCA algorithm to accelerate the training process. DeLi-CoCo (Hashemi et al., 2022) performs multiple compression gossip steps in each iteration for fast convergence with arbitrary communication compression. Network-DANE (Li et al., 2020a) uses multiple gossip steps and generalizes DANE to decentralized scenarios. In general, by increasing the number of gossip steps, local clients can reach a better consensus model to improve the performance of CFL. However, MGS has yet to be explored to mitigate the model inconsistency in the DFL setting.

The work most related to this paper is DFedAvg and DFedAvg with momentum (DFedAvgM) in Sun et al. (2022), which leverage multiple local iterations with the SGD optimizer and significantly improve the performance of classic decentralized parallel SGD method D-PSGD (Lian et al., 2017). However, DFL may still suffer from inferior performance due to the severe model inconsistency among clients. Another related work is FedSAM (Qu et al., 2022), which integrates SAM into CFL to enhance the flatness of local model and achieves new SOTA performance for CFL. On top of the aforementioned studies, we extend the SAM optimizer to the DFL setting and simultaneously provide its convergence guarantee in the nonconvex setting. Furthermore, we bridge the gap between CFL and DFL via adopting MGS in DFedSAM-MGS, which largely mitigates the model inconsistency in DFL.

3. Methodology

In this section, we introduce the problem setting in DFL and present the details of the proposed DFedSAM and DFedSAM-MGS.

3.1. Problem Setting

In this work, we are interested in solving the following finite-sum stochastic non-convex minimization problem:

$$\min_{\mathbf{x} \in \mathbb{R}^d} f(\mathbf{x}) := \frac{1}{m} \sum_{i=1}^m f_i(\mathbf{x}), \quad f_i(\mathbf{x}) = \mathbb{E}_{\xi \sim \mathcal{D}_i} F_i(\mathbf{x}; \xi), \quad (1)$$

where \mathcal{D}_i denotes the data distribution in the i -th client, which is heterogeneous across clients; m is the number of clients, and $F_i(\mathbf{x}; \xi)$ is the local objective function associated with the training data samples ξ . Equation (1) is known as the empirical risk minimization (ERM) with many applications in ML. As shown in Figure 1(b), the communication network in the decentralized network topology between clients is modeled as an undirected connected graph $\mathcal{G} = (\mathcal{N}, \mathcal{V}, \mathbf{W})$, where $\mathcal{N} = \{1, 2, \dots, m\}$ represents the set of clients, and $\mathcal{V} \subseteq \mathcal{N} \times \mathcal{N}$ represents the set

of communication channels, each connecting two distinct clients. Furthermore, there is no central server in the decentralized setting and all clients only communicate with their neighbors via the communication channels \mathcal{V} . In addition, we assume that Equation (1) is well-defined and denote f^* as the minimal value of f : $f(x) \geq f(x^*) = f^*$ for all $x \in \mathbb{R}^d$.

Algorithm 1 DFedSAM and DFedSAM-MGS

Input : Total number of clients m , total number of communication rounds T , the number of consensus steps per gradient iteration Q , learning rate η , and total number of the local iterates are K .

Output : The consensus model \mathbf{x}^T after the final communication of all clients.

```

1 Initialization: Randomly initialize each model  $\mathbf{x}^0(i)$ .
   for  $t = 0$  to  $T - 1$  do
2     for node  $i$  in parallel do
3       for  $k = 0$  to  $K - 1$  do
4         Set  $\mathbf{y}^{t,0}(i) \leftarrow \mathbf{x}^t(i)$ ,  $\mathbf{y}^{t,-1}(i) = \mathbf{y}^{t,0}(i)$ 
           Sample a batch of local data  $\xi_i$  and calculate local
           gradient  $\mathbf{g}^{t,k}(i) = \nabla F_i(\mathbf{y}^{t,k}; \xi_i)$ 
            $\tilde{\mathbf{g}}^{t,k}(i) = \nabla F_i(\mathbf{y}^{t,k} + \delta(\mathbf{y}^{t,k}); \xi_i)$  with  $\delta(\mathbf{y}^{t,k}) =$ 
            $\rho \mathbf{g}^{t,k} / \|\mathbf{g}^{t,k}\|_2$ 
            $\mathbf{y}^{t,k+1}(i) = \mathbf{y}^{t,k}(i) - \eta \tilde{\mathbf{g}}^{t,k}(i)$ 
5       end
6      $\mathbf{z}^t(i) \leftarrow \mathbf{y}^{t,K}(i)$ 
           Receive neighbors' models  $\mathbf{z}^t(l)$  from neighborhood set
            $\mathcal{S}_{k,t}$  with adjacency matrix  $\mathbf{W}$ .
            $\mathbf{x}^{t+1}(i) = \sum_{l \in \mathcal{N}(i)} w_{i,l} \mathbf{z}^t(l)$ 
7     for  $q = 0$  to  $Q - 1$  do
            $\mathbf{x}^{t,q+1}(i) = \sum_{l \in \mathcal{N}(i)} w_{i,l} \mathbf{z}^{t,q}(l)$  ( $\mathbf{z}^{t,0}(i) = \mathbf{z}^t(i)$ )
            $\mathbf{z}^{t,q+1}(i) = \mathbf{x}^{t,q+1}(i)$ 
8     end
9      $\mathbf{x}^{t+1}(i) = \mathbf{x}^{t,Q}(i)$ 
10  end
11 end
    
```

3.2. DFedSAM and DFedSAM-MG

Instead of searching for a solution via SGD (Bottou, 2010; Bottou et al., 2018), SAM (Foret et al., 2021) aims to seek a solution in a flat region by adding a small perturbation to the models, i.e., $x + \delta$ with more robust performance. As shown in Figure 2, the decentralized scheme has a sharper landscape with poorer generalization ability compared with the centralized scheme. However, the study focused on this issue remains unexplored. In this paper, we incorporate the SAM optimizer into DFL to explore this feature, and the local loss function of the proposed DFedSAM is defined as:

$$f_i(\mathbf{x}) = \mathbb{E}_{\xi \sim \mathcal{D}_i} \max_{\|\delta_i\|_2 \leq \rho} F_i(\mathbf{y}^{t,k}(i) + \delta_i; \xi_i), \quad i \in \mathcal{N} \quad (2)$$

where $\mathbf{y}^{t,k}(i) + \delta_i$ is the perturbed model, and ρ is a pre-defined constant controlling the radius of the perturbation and $\|\cdot\|_2$ is a l_2 -norm, which is simplified to $\|\cdot\|$ in the rest. Similar to CFL methods, in DFedSAM, clients can update local model parameters with multiple local iterates before conducting communication. Specifically, for each client $i \in \{1, 2, \dots, m\}$, in each local iteration $k \in \{0, 1, \dots, K-1\}$ and each communication round $t \in \{0, 1, \dots, T-1\}$, the k -th inner iteration in client i is performed as:

$$\mathbf{y}^{t,k+1}(i) = \mathbf{y}^{t,k}(i) - \eta \tilde{\mathbf{g}}^{t,k}(i), \quad (3)$$

where $\tilde{\mathbf{g}}^{t,k}(i) = \nabla F_i(\mathbf{y}^{t,k} + \delta(\mathbf{y}^{t,k}); \xi)$, $\delta(\mathbf{y}^{t,k}) = \rho \mathbf{g}^{t,k} / \|\mathbf{g}^{t,k}\|_2$, and using first order Taylor expansion around $\mathbf{y}^{t,k}$ for a small value of ρ (Foret et al., 2021). After K inner iterations in each client, parameters are updated as $\mathbf{z}^t(i) \leftarrow \mathbf{y}^{t,K}(i)$ and sent to its neighbors $l \in \mathcal{N}(i)$ after local updates. Then, each client averages its parameters with the information of its neighbors (including itself):

$$\mathbf{x}^{t+1}(i) = \sum_{l \in \mathcal{N}(i)} w_{i,l} \mathbf{z}^t(l). \quad (4)$$

Furthermore, we employ the multiple gossip steps (MGS) technique (Ye et al., 2020; Ye & Zhang, 2021; Hashemi et al., 2022) to achieve better consistency among local models, named DFedSAM-MGS, to ensure a balance between the communication cost and generalization ability in DFL. Specifically, the generation of MGS at the q -th step ($q \in \{0, 1, \dots, Q-1\}$) can be viewed as two steps in terms of exchanging messages and local gossip update as follows:

$$\mathbf{x}^{t,q+1}(i) = \sum_{l \in \mathcal{N}(i)} w_{i,l} \mathbf{z}^{t,q}(l), \text{ and } \mathbf{z}^{t,q+1}(i) = \mathbf{x}^{t,q+1}(i). \quad (5)$$

At the end of MGS, $\mathbf{x}^{t+1}(i) = \mathbf{x}^{t,Q}(i)$. Our proposed algorithms are summarized in Algorithm 1. It is clear that, in DFedSAM, there is a trade-off between the local computation complexity and communication overhead via multiple local iterations, whereas the local communication is only performed at once. By contrast, DFedSAM-MGS performs multiple local communications with a larger Q to make all local clients synchronized. Therefore, DFedSAM-MGS can be viewed as a compromise between DFL and CFL.

Compared with existing SOTA DFL methods: DFedAvg and DFedAvgM (Sun et al., 2022), the benefits of DFedSAM and DFedSAM-MGS lie in three-fold: (i) SAM is introduced to first alleviate the local over-fitting issue caused by the inconsistency among local models via seeking a flat model at each client in DFL, and can also help make the consensus model flat; (ii) In DFedSAM-MGS, MGS is used to further accelerate the aggregation of local flatness models

for better consistency among local models based on DFedSAM and properly balance the communication complexity and learning performance; (iii) Furthermore, we also present the theories unifying the impacts of gradient perturbation ρ in SAM, several times of local communications Q in MGS, and various network typologies λ , along with data homogeneity β upon the convergence rate in Section 4.

4. Convergence Analysis

In this section, we show the convergence results of DFedSAM and DFedSAM-MGS for general non-convex FL setting, and the detailed proof is presented in Appendix D. Below, we first give several useful and necessary notations and assumptions.

Definition 4.1. (The gossip/mixing matrix). [Definition 1, (Sun et al., 2022)] The gossip matrix $\mathbf{W} = [w_{i,j}] \in [0, 1]^{m \times m}$ is assumed to have these properties: (i) (**Graph**) If $i \neq j$ and $(i, j) \notin \mathcal{V}$, then $w_{i,j} = 0$, otherwise, $w_{i,j} > 0$; (ii) (**Symmetry**) $\mathbf{W} = \mathbf{W}^\top$; (iii) (**Null space property**) $\text{null}\{\mathbf{I} - \mathbf{W}\} = \text{span}\{\mathbf{1}\}$; (iv) (**Spectral property**) $\mathbf{I} \succeq \mathbf{W} \succ -\mathbf{I}$. Under these properties, eigenvalues of \mathbf{W} can be shown satisfying $1 = |\lambda_1(\mathbf{W})| > |\lambda_2(\mathbf{W})| \geq \dots \geq |\lambda_m(\mathbf{W})|$. Furthermore, $\lambda := \max\{|\lambda_2(\mathbf{W})|, |\lambda_m(\mathbf{W})|\}$ and $1 - \lambda \in (0, 1]$ is the denoted as spectral gap of \mathbf{W} .

Definition 4.2. (Homogeneity parameter). [Definition 2, (Li et al., 2020a)] For any $i \in \{1, 2, \dots, m\}$ and the parameter $\mathbf{x} \in \mathbb{R}^d$, the homogeneity parameter β can be defined as:

$$\beta := \max_{1 \leq i \leq m} \beta_i, \text{ with } \beta_i := \sup_{\mathbf{x} \in \mathbb{R}^d} \|\nabla f_i(\mathbf{x}) - \nabla f(\mathbf{x})\|.$$

Assumption 4.3. (Lipschitz smoothness). The function f_i is differentiable and ∇f_i is L -Lipschitz continuous, $\forall i \in \{1, 2, \dots, m\}$, i.e., $\|\nabla f_i(\mathbf{x}) - \nabla f_i(\mathbf{y})\| \leq L\|\mathbf{x} - \mathbf{y}\|$, for all $\mathbf{x}, \mathbf{y} \in \mathbb{R}^d$.

Assumption 4.4. (Bounded variance). The gradient of the function f_i have σ_l -bounded variance, i.e.,

$$\mathbb{E}_{\xi_i} \|\nabla F_i(\mathbf{y}; \xi_i) - \nabla f_i(\mathbf{x})\|^2 \leq \sigma_l^2, \forall i \in \{1, 2, \dots, m\},$$

the global variance is also bounded, i.e., $\frac{1}{m} \sum_{i=1}^m \|\nabla f_i(\mathbf{x}) - \nabla f(\mathbf{x})\|^2 \leq \sigma_g^2$ for all $\mathbf{x} \in \mathbb{R}^d$. It is not hard to verify that the σ_g is smaller than the homogeneity parameter β , i.e., $\sigma_g^2 \leq \beta^2$.

Note that above mentioned assumptions are mild and commonly used in characterizing the convergence rate of FL (Sun et al., 2022; Ghadimi & Lan, 2013; Yang et al., 2021; Bottou et al., 2018; Yu et al., 2019; Reddi et al., 2021). Compared with classic decentralized parallel SGD methods such as D-PSGD (Lian et al., 2017), the technical difficulty is that $\mathbf{z}^t(i) - \mathbf{x}^t(i)$ fails to be an unbiased gradient estimation

$\nabla f_i(\mathbf{x}^t(i))$ after multiple local iterates, thereby merging the multiple local iterations is non-trivial. Furthermore, the various topologies of communication networks in DFL are quite different with SAM in CFL (Qu et al., 2022). Below, we adopt the averaged parameter $\bar{\mathbf{x}}^t = \frac{1}{m} \sum_{i=1}^m \mathbf{x}^t(i)$ of all clients to be the approximated solution of Problem (1).

Theorem 4.5. *Let Assumptions 4.3 and 4.4 hold, and the parameters $\{\mathbf{x}^t(i)\}_{t \geq 0}$ is generated via Algorithm 1. Meanwhile, assume the learning rate of SAM in each client satisfy $0 < \eta \leq \frac{1}{10KL}$. Let $\bar{\mathbf{x}}^t = \frac{1}{m} \sum_{i=1}^m \mathbf{x}^t(i)$ and denote $\Phi(\lambda, m, Q)$ as the metric related with three parameters in terms of the number of spectral gap, the clients and multiple gossip steps,*

$$\Phi(\lambda, m, Q) = \frac{\lambda^Q + 1}{(1 - \lambda)^2 m^{2(Q-1)}} + \frac{\lambda^Q + 1}{(1 - \lambda^Q)^2}, \quad (6)$$

Then, we have the gradient estimation of DFedSAM or DFedSAM-MGS for solving Problem (1):

$$\min_{1 \leq t \leq T} \mathbb{E} \|\nabla f(\bar{\mathbf{x}}^t)\|^2 \leq \frac{2[f(\bar{\mathbf{x}}^1) - f^*]}{T(\eta K - 32\eta^3 K^2 L^2 - 6\eta^2 KL)} \quad (7)$$

$$+ \alpha(K, \rho, \eta) + \Phi(\lambda, m, Q)\beta(K, \rho, \eta),$$

where T is the number of communication rounds and the constants are given as

$$\alpha(K, \rho, \eta) = \frac{\eta KL}{2(\eta K - 32\eta^3 K^2 L^2 - 6\eta^2 KL)} \left(2KL \left(\frac{4K^3 L^2 \eta^2 \rho^4}{2K - 1} \right. \right.$$

$$\left. \left. + 8K\eta^2(L^2 \rho^2 + \sigma_g^2 + \sigma_i^2) + \frac{\rho^2}{2K - 1} \right) + \eta(L^2 \rho^2 + \sigma_i^2) \right),$$

$$\beta(K, \rho, \eta) = \frac{\eta^4 KL^3(16\eta KL + 3)}{\eta K - 32\eta^3 K^2 L^2 - 6\eta^2 KL} \left(2K \left(\frac{4K^3 L^2 \rho^4}{2K - 1} \right. \right.$$

$$\left. \left. + 8K(L^2 \rho^2 + \sigma_g^2 + \sigma_i^2) \right) + \frac{2K\rho^2}{\eta^2(2K - 1)} \right).$$

With Theorem 4.5, we state the following convergence rates for DFedSAM and DFedSAM-MGS.

Corollary 4.6. *Let the local adaptive learning rate satisfy $\eta = \mathcal{O}(1/L\sqrt{KT})$. With the similar assumptions required in Theorem 4.6, and setting the perturbation parameter $\rho = \mathcal{O}(\frac{1}{\sqrt{T}})$. Then, the convergence rate for DFedSAM satisfies:*

$$\min_{1 \leq t \leq T} \mathbb{E} \|\nabla f(\bar{\mathbf{x}}^t)\|^2 = \mathcal{O} \left(\frac{(f(\bar{\mathbf{x}}^1) - f^*) + \sigma_i^2}{\sqrt{KT}} + \frac{K(\beta^2 + \sigma_i^2)}{T} \right.$$

$$\left. + \frac{L^2}{K^{1/2}T^{3/2}} + \frac{\beta^2 + \sigma_i^2}{K^{1/2}T^{3/2}(1 - \lambda)^2} \right).$$

Remark 4.7. Due to the effect of the radius of the perturbation ρ by using SAM, DFedSAM can achieve a better bound than the state-of-the-art (SOTA) bounds such as $\mathcal{O}\left(\frac{1}{\sqrt{T}} + \frac{\sigma_g^2}{\sqrt{T}} + \frac{\sigma_g^2 + B^2}{(1 - \lambda)^2 T^{3/2}}\right)$ in (Sun et al., 2022), where B is the upper bound of the gradient. And the reason

behind this is that the diverse impact of various communication topologies λ on convergence rate can be alleviated by the effect of the radius of the perturbation ρ , i.e., $\rho = \mathcal{O}(\frac{1}{\sqrt{T}})$ (we set $\rho = 0.01$ when $T = 1000$). Note that the bound can be tighter as λ decreases, which is dominated by $\frac{\beta^2 + \sigma_i^2}{K^{1/2}T^{3/2}(1 - \lambda)^2}$ terms as $\lambda \geq 1 - \frac{1}{\sqrt{T}}$, whereas as β increases, it can be degraded. Furthermore, when the smoothness is not good, which means that L is large. The additional term $\mathcal{O}(\frac{L^2}{K^{1/2}T^{3/2}})$ can be neglected compared to other terms, which comes from the additional SGD step for smoothness via SAM local optimizer.

Corollary 4.8. *Let $Q > 1$, T be large enough and $\eta = \mathcal{O}(1/L\sqrt{KT})$. With the similar assumptions required in Theorem 4.6 and perturbation amplitude ρ being $\rho = \mathcal{O}(\frac{1}{\sqrt{T}})$. Then, the convergence rate for DFedSAM-MGS satisfies:*

$$\min_{1 \leq t \leq T} \mathbb{E} \|\nabla f(\bar{\mathbf{x}}^t)\|^2 = \mathcal{O} \left(\frac{(f(\bar{\mathbf{x}}^1) - f^*) + \sigma_i^2}{\sqrt{KT}} + \frac{K(\beta^2 + \sigma_i^2)}{T} \right.$$

$$\left. + \frac{L^2}{K^{1/2}T^{3/2}} + \Phi(\lambda, m, Q) \frac{\beta^2 + \sigma_i^2}{K^{1/2}T^{3/2}} \right).$$

Remark 4.9. The impact of the network topology $(1 - \lambda)$ can be alleviated as Q increases and the number of clients m is large enough, the term $\frac{\lambda^Q + 1}{(1 - \lambda)^2 m^{2(Q-1)}}$ of $\Phi(\lambda, m, Q)$ can be neglected, and the term $\frac{\lambda^Q + 1}{(1 - \lambda^Q)^2}$ is close to 1. That means by using the proposed Q -step gossip procedure, model consistency among clients can be improved, and thus DFL in the various communication topologies can be roughly viewed as CFL. Thus, the negative effect of the gradient variances σ_i^2 and β^2 can be degraded especially on sparse network topology where λ is close to 1. In practice, a suitable steps $Q > 1$ is possible to achieve a communication-accuracy trade-off in DFL.

Remark 4.10. Note that $\Phi(\lambda, m, Q)$ is $\frac{2(\lambda+1)}{(1-\lambda)^2} \leq \frac{4}{(1-\lambda)^2}$ if $Q = 1$. And the result is the same as Corollary 4.6.

5. Experiments

In this section, we evaluate the efficacy of our algorithms compared to six baselines from CFL and DFL settings. In addition, we conduct several experiments to verify the impact of the communication network topology in Section 4. Furthermore, several ablation studies are conducted.

5.1. Experiment Setup

Dataset and Data Partition. The efficacy of the proposed DFedSAM and DFedSAM-MGS is evaluated on CIFAR-10 and CIFAR-100 datasets (Krizhevsky et al., 2009) in both IID and non-IID settings. Specifically, Dir Partition (Hsu et al., 2019) is used for simulating non-IID across federated clients, where the local data of each client is partitioned by splitting the total dataset through sampling the label

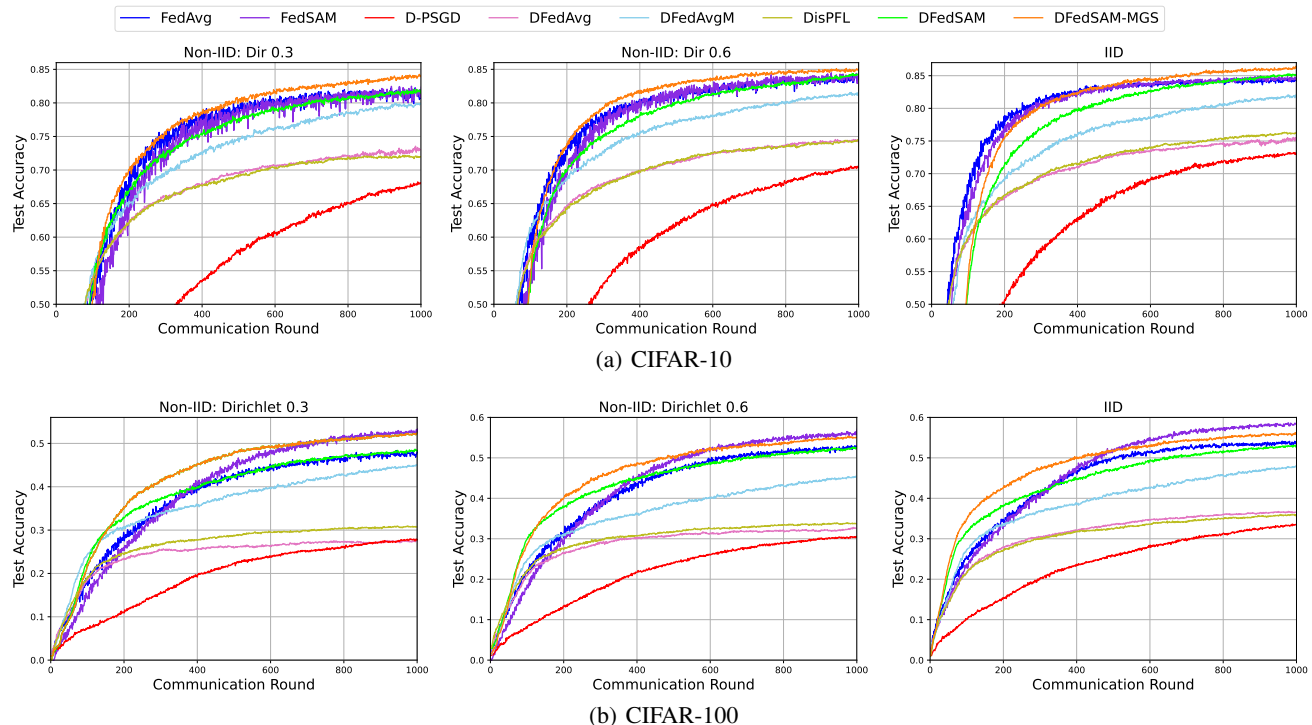


Figure 3. Test accuracy of all baselines from both CFL and DFL with (a) CIFAR-10 and (b) CIFAR-100 in both IID and non-IID settings.

ratios from the Dirichlet distribution $\text{Dir}(\alpha)$ with parameters $\alpha = 0.3$ and $\alpha = 0.6$.

Baselines. The compared baselines cover several SOTA methods in both the CFL and DFL settings. Specifically, centralized baselines include FedAvg (McMahan et al., 2017) and FedSAM (Qu et al., 2022). For decentralized setting, D-PSGD (Lian et al., 2017), DFedAvg and DFedAvgM (Sun et al., 2022), along with DisPFL (Dai et al., 2022), are used for comparison.

Implementation Details. The total number of clients is set as 100, among which 10% clients participates in communication. Specifically, all clients perform the local iteration step for decentralized methods and only participated clients can perform local update for centralized methods. We initialize the local learning rate as 0.1 with a decay rate 0.998 per communication round for all experiments. For CIFAR-10 and CIFAR-100 datasets, VGG-11 (He et al., 2016) and ResNet-18 (Simonyan & Zisserman, 2014) are adopted as the backbones in each client, respectively. The number of communication rounds is set as 1000 in the experiments for comparing with all baselines and studying on topology-aware performance. In addition, all the ablation studies are conducted on CIFAR-10 dataset and the number of communication rounds is set as 500.

Communication Configurations. For a fair comparison between decentralized and centralized setting, we apply a dynamic time-varying connection topology for decentral-

ized methods to ensure that in each round, the number of connections are no more than that in the central server. In specific, the number of clients communicating with their neighbors can be controlled to keep the communication volume consistent with centralized methods. Following earlier works, the communication complexity is measured by the times of local communications. Furthermore, the setup of the more detailed experiment are presented in Appendix B due to the limited space.

5.2. Performance Evaluation

Performance with compared baselines. In Table 1 and Figure 3, we evaluate DFedSAM and DFedSAM-MGS ($Q = 4$) with $\rho = 0.01$ on CIFAR-10 and CIFAR-100 datasets in both settings compared with all baselines from CFL and DFL. From these results, it is clearly seen that our proposed algorithms outperform other decentralized methods on this two datasets, and DFedSAM-MGS outperforms and roughly achieves the performance of SOTA centralized baseline FedSAM on CIFAR-10 and CIFAR-100, respectively. Specifically, the training accuracy and testing accuracy are presented in Table 1 to show the generalization performance. We can see that the performance improvement is more obvious than all other baselines on CIFAR-10 with the same communication round. For instance, the difference between training accuracy and test accuracy on CIFAR-10 in IID setting is 14.14% in DFedSAM, 13.22% in DFedSAM-MGS, 15.29% in FedAvg and

Table 1. Train accuracy (%) and test accuracy (%) on two datasets in both IID and non-IID settings.

Algorithm	CIFAR-10						CIFAR-100					
	Dirichlet 0.3		Dirichlet 0.6		IID		Dirichlet 0.3		Dirichlet 0.6		IID	
	Train	Validation	Train	Validation	Train	Validation	Train	Validation	Train	Validation	Train	Validation
FedAvg	99.99	82.39	99.99	84.17	99.99	84.70	99.99	48.36	99.99	53.06	99.99	54.16
FedSAM	99.75	82.49	99.89	85.04	99.98	84.98	99.99	51.98	99.99	54.88	99.99	59.60
D-PSGD	98.59	68.23	99.09	70.58	99.75	73.23	90.72	27.98	90.15	30.62	92.19	33.64
DFedAvg	99.75	73.55	99.93	74.67	99.95	75.55	99.56	27.62	99.56	32.82	99.68	36.77
DFedAvgM	99.93	79.96	99.95	81.56	99.95	82.07	99.56	45.11	99.60	45.50	99.78	47.98
DisPFL	99.90	72.19	99.93	74.43	99.95	85.30	97.20	30.15	99.48	32.44	99.69	35.98
DFedSAM	99.41	82.04	99.44	84.38	99.44	85.30	99.87	48.66	99.85	50.70	99.97	53.12
DFedSAM-MGS	99.53	84.26	99.65	85.14	99.69	86.47	99.92	52.37	99.95	54.91	99.97	56.15

15% in FedSAM. That means our algorithms achieve a comparable generalization to centralized baselines. In general, the upper-performance limitation of DFedSAM is consistent with FedSAM, after all, they apply different optimizer algorithms to solve the same optimization problem.

Impact of non-IID levels (β). In Table 1, we can see our algorithms are robust to different participation cases. Heterogeneous data distribution of local client is set to various participation levels from IID, Dirichlet 0.6 and Dirichlet 0.3, which makes the training of global/consensus model is more difficult. For instance, on CIFAR-10, as non-IID levels increases, DFedSAM-MGS achieves better generalization than FedSAM as the difference between training accuracy and test accuracy in DFedSAM-MGS {15.27%, 14.51%, 13.22%} are lower than that in FedSAM {17.26%, 14.85%, 15%}. Similarly, the difference in DFedSAM {17.37%, 15.06%, 14.10%} are lower than that in FedAvg {17.60%, 15.82%, 15.27%}. These observations confirm that our algorithms are more robust than baselines in various degrees of heterogeneous data.

5.3. Topology-aware Performance

We verify the influence of various communication topologies and gossip averaging steps in DFedSAM and DFedSAM-MGS. Different with the comparison of CFL and DFL in Section 5.2, we only need to verify the key properties for the DFL methods in this section. Thus, the communication type is set as ‘‘Complete’’, i.e., each client can communicate with its neighbors in the same communication round.

Table 2. Testing accuracy (%) in various network topologies compared with decentralized algorithms on CIFAR-10.

Algorithm	Ring	Grid	Exponential	Full-connected
D-PSGD	68.96	74.36	74.90	75.35
DFedAvg	69.95	80.17	83.13	83.48
DFedAvgM	72.55	85.24	86.94	87.50
DFedSAM	73.19 \uparrow	85.28 \uparrow	87.44 \uparrow	88.05 \uparrow
DFedSAM-MGS	80.55 \uparrow	87.39 \uparrow	88.06 \uparrow	88.20 \uparrow

The degree of sparse connectivity λ is: ring > grid > expo-

nenial > full-connected in DFL. From Table 2, our algorithms are obviously superior to all decentralized baselines in various communication networks, which is coincided with our theoretical findings. Specifically, compared with DFedAvgM, DFedSAM and DFedSAM-MGS can significantly improve the performance in the ring topology with 0.64% and 8.0%, respectively. Meanwhile, the performance of DFedSAM-MGS in various topologies is always better than that of other methods. This observation confirms that multiple gossip steps Q can alleviate the impact of network topology with a smaller $Q = 4$. Therefore, our algorithms can generate the better generalization and model consistency in various communication topologies.

5.4. Ablation Study

Below, we verify the influence of each component and hyperparameter in DFedSAM where $Q = 1$. All the ablation studies are conducted in ‘‘exponential’’ topology except the study for Q in three topologies, and the communication type is the same as Section 5.3: ‘‘Complete’’.

Consensus/gossip steps Q . In Figure 4, we investigate where the balance between learning performance and communication complexity in three network topologies is. In general, larger Q can better solve the local consistency problem, but it also introduces additional communication cost. In the decentralized training setting, it is easier to obtain an optimal Q . Thus, we only treat Q as a hyperparameter in our experiments and study the different balance points on different values of $1 \leq Q \leq 4$ under the various communication topologies in Figure 4 (a), (b) and (c), such as ring, grid, and exponential. As the number of local communications increases, model performance is also improved but the communication complexity increases too. It is clearly seen that the balance point is different but with the same tendency in different topologies. And a relatively larger Q can bring better performance for a given communication complexity. Therefore, we select $Q = 4$ in DFedSAM-MGS under 1000 communication rounds for a better balance.

Local iteration steps K . Large local iteration steps K can help the convergence in previous DFL work (Sun et al.,

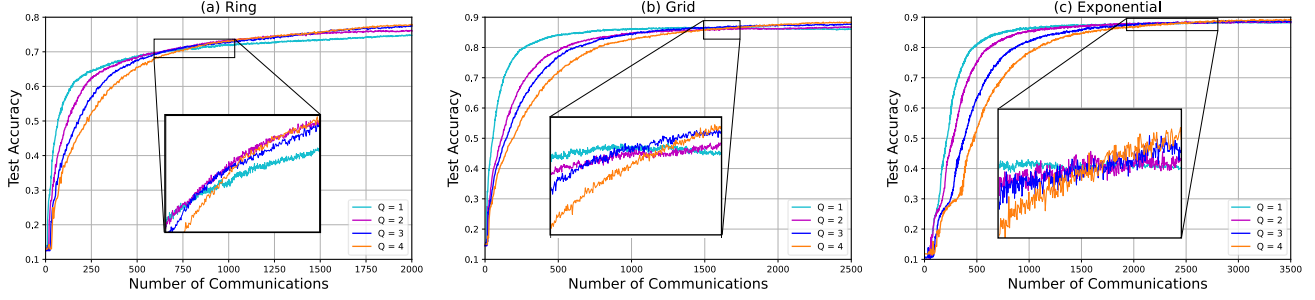


Figure 4. Test accuracy with the number of local communications in various values of Q .

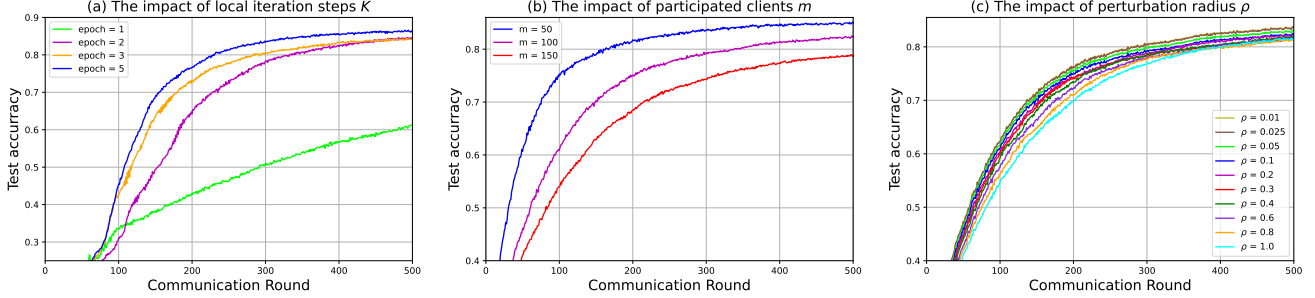


Figure 5. Impact of hyper-parameters: local iteration steps K , participated clients m , perturbation radius ρ .

2022) with the theoretical guarantees. To investigate the acceleration on T by adopting a larger local iteration steps K , we fix the total batchsize and change local training epochs. As shown in Figure 5 (a), our algorithms can accelerate the convergence in theoretical results (see Section 4.5) as a larger local iteration steps K is adopted.

Number of participated clients m . As shown in Figure 5 (b), we compare the performance between different number of client participation $m = \{50, 100, 150\}$ with the same hyper-parameters. Compared with larger $m = 150$, the smaller $m = \{50, 100\}$ can achieve better convergence and test accuracy as the number of local data increases. We can find that the small client size has better training performance due to more samples in each client and the relationship between training performance and client size is approximately linear.

Perturbation radius ρ . Perturbation radius ρ has the impact on performance as the adding perturbation is accumulated when the communication round T increases. It is a trade-off between test accuracy and the generalization. To select a proper value for our algorithms, we conduct some experiments on various perturbation radius from the set $\{0.01, 0.025, 0.05, 0.1, 0.2, 0.4, 0.6, 0.8, 1.0\}$ in Figure 5 (c). As $\rho = 0.01$, we achieve a better convergence and performance. Meanwhile, $\rho = \mathcal{O}(\frac{1}{\sqrt{T}})$ can make a linear speedup on convergence (see Section 4.5).

The effectiveness of SAM and MGS. To validate the effectiveness of SAM and MGS, respectively, we compare four

Table 3. Test accuracy of DFedAvg and DFedSAM along with DFedSAM-MGS.

Algorithm	Train (%)	Validation (%)	Differential value (%)
DFedAvg	98.86	82.10	16.76
DFedSAM	92.26	84.70 \uparrow	7.56 \downarrow
DFedSAM-MGS	92.55	85.56 \uparrow	6.99 \downarrow

algorithms including DFedAvg, DFedSAM and FedSAM-MGS with the same setting. From Table 3, DFedSAM can achieve the performance improvement and better generalization compared with DFedAvg as SAM optimizer is adopted. DFedSAM-MGS can further boost the performance compared with FedSAM as MGS can also make models consistent among clients and accelerate the convergence rates.

6. Conclusions And Future Work

In this paper, we focus on the model inconsistency challenge caused by heterogeneous data and network connectivity of communication topology in DFL and overcome this challenge from the perspectives of model generalization. We propose two DFL frameworks: DFedSAM and DFedSAM-MGS with better model consistency among clients. DFedSAM adopts SAM to achieve the flatness model in each client, thereby improving the generalization by generating a consensus/global flatness model. And DFedSAM-MGS further improves the model consistency based on DFedSAM by accelerating the aggregation of local flat models and reaching a better trade-off between learning performance and communication complexity. For theoretical findings, we

confirm a linear speedup and unify the impacts of gradient perturbation in SAM, local communications in MGS, and network topology, along with data homogeneity upon the convergence rate in DFL. Furthermore, empirical results also verify the superiority of our approaches. For future work, we will continue towards understanding of the effect of SAM and MGS for more desirable generalization in DFL.

References

- Abbas, M., Xiao, Q., Chen, L., Chen, P., and Chen, T. Sharp-maml: Sharpness-aware model-agnostic meta learning. In *International Conference on Machine Learning, ICML*, pp. 10–32, 2022.
- Acar, D. A. E., Zhao, Y., Navarro, R. M., Mattina, M., Whatmough, P. N., and Saligrama, V. Federated learning based on dynamic regularization. In *9th International Conference on Learning Representations, ICLR*, 2021.
- Andriushchenko, M. and Flammarion, N. Towards understanding sharpness-aware minimization. In *International Conference on Machine Learning, ICML*, Proceedings of Machine Learning Research, pp. 639–668. PMLR, 2022.
- Bottou, L. Large-scale machine learning with stochastic gradient descent. In *Proceedings of COMPSTAT'2010*, pp. 177–186. Springer, 2010.
- Bottou, L., Curtis, F. E., and Nocedal, J. Optimization methods for large-scale machine learning. *Siam Review*, 60(2):223–311, 2018.
- Caldarola, D., Caputo, B., and Ciccone, M. Improving generalization in federated learning by seeking flat minima. *CoRR*, abs/2203.11834, 2022.
- Dai, R., Shen, L., He, F., Tian, X., and Tao, D. Dispf: Towards communication-efficient personalized federated learning via decentralized sparse training. In *International Conference on Machine Learning, ICML*, Proceedings of Machine Learning Research, pp. 4587–4604. PMLR, 2022.
- Du, J., Yan, H., Feng, J., Zhou, J. T., Zhen, L., Goh, R. S. M., and Tan, V. Efficient sharpness-aware minimization for improved training of neural networks. In *International Conference on Learning Representations*, 2021.
- Foret, P., Kleiner, A., Mobahi, H., and Neyshabur, B. Sharpness-aware minimization for efficiently improving generalization. In *International Conference on Learning Representations*, 2021.
- Ghadimi, S. and Lan, G. Stochastic first-and zeroth-order methods for nonconvex stochastic programming. *SIAM Journal on Optimization*, 23(4):2341–2368, 2013.
- Hashemi, A., Acharya, A., Das, R., Vikalo, H., Sanghavi, S., and Dhillon, I. On the benefits of multiple gossip steps in communication-constrained decentralized federated learning. *IEEE Transactions on Parallel and Distributed Systems, TPDS*, pp. 2727–2739, 2022.
- He, K., Zhang, X., Ren, S., and Sun, J. Deep residual learning for image recognition. In *Proceedings of the IEEE conference on computer vision and pattern recognition*, pp. 770–778, 2016.
- Hsu, T.-M. H., Qi, H., and Brown, M. Measuring the effects of non-identical data distribution for federated visual classification. *arXiv preprint arXiv:1909.06335*, 2019.
- Kairouz, P., McMahan, H. B., Avent, B., Bellet, A., Bennis, M., Bhagoji, A. N., Bonawitz, K., Charles, Z., Cormode, G., Cummings, R., et al. Advances and open problems in federated learning. *Foundations and Trends in Machine Learning*, pp. 1–210, 2021.
- Karimireddy, S. P., Kale, S., Mohri, M., Reddi, S., Stich, S., and Suresh, A. T. Scaffold: Stochastic controlled averaging for federated learning. In *International Conference on Machine Learning*, pp. 5132–5143. PMLR, 2020.
- Krizhevsky, A., Hinton, G., et al. Learning multiple layers of features from tiny images. 2009.
- Kwon, J., Kim, J., Park, H., and Choi, I. K. Asam: Adaptive sharpness-aware minimization for scale-invariant learning of deep neural networks. In *International Conference on Machine Learning*, pp. 5905–5914. PMLR, 2021.
- Lalitha, A., Shekhar, S., Javidi, T., and Koushanfar, F. Fully decentralized federated learning. In *Third workshop on Bayesian Deep Learning (NeurIPS)*, 2018.
- Lalitha, A., Kilinc, O. C., Javidi, T., and Koushanfar, F. Peer-to-peer federated learning on graphs. *arXiv preprint arXiv:1901.11173*, 2019.
- Li, B., Cen, S., Chen, Y., and Chi, Y. Communication-efficient distributed optimization in networks with gradient tracking and variance reduction. *Journal of Machine Learning Research, JMLR*, pp. 180:1–180:51, 2020a.
- Li, H., Xu, Z., Taylor, G., Studer, C., and Goldstein, T. Visualizing the loss landscape of neural nets. *Advances in neural information processing systems*, 31, 2018.
- Li, T., Sahu, A. K., Talwalkar, A., and Smith, V. Federated learning: Challenges, methods, and future directions. *IEEE Signal Processing Magazine*, pp. 50–60, 2020b.
- Li, T., Sahu, A. K., Zaheer, M., Sanjabi, M., Talwalkar, A., and Smith, V. Federated optimization in heterogeneous networks. *Proceedings of Machine Learning and Systems*, pp. 429–450, 2020c.

- Lian, X., Zhang, C., Zhang, H., Hsieh, C.-J., Zhang, W., and Liu, J. Can decentralized algorithms outperform centralized algorithms? a case study for decentralized parallel stochastic gradient descent. In *Advances in Neural Information Processing Systems*, pp. 5330–5340, 2017.
- Liu, Y., Mai, S., Chen, X., Hsieh, C.-J., and You, Y. Towards efficient and scalable sharpness-aware minimization. In *Proceedings of the IEEE/CVF Conference on Computer Vision and Pattern Recognition*, pp. 12360–12370, 2022.
- McMahan, H. B., Moore, E., Ramage, D., Hampson, S., and Arcas, B. A. Y. Communication-efficient learning of deep networks from decentralized data. pp. 1273–1282, 2017.
- Nedic, A. and Ozdaglar, A. Distributed subgradient methods for multi-agent optimization. *IEEE Transactions on Automatic Control*, 54(1):48–61, 2009.
- Qu, Z., Li, X., Duan, R., Liu, Y., Tang, B., and Lu, Z. Generalized federated learning via sharpness aware minimization. In *International Conference on Machine Learning, ICML*, pp. 18250–18280, 2022.
- Reddi, S. J., Charles, Z., Zaheer, M., Garrett, Z., Rush, K., Konečný, J., Kumar, S., and McMahan, H. B. Adaptive federated optimization. In *International Conference on Learning Representations*, 2021. URL <https://openreview.net/forum?id=LkFG3lB13U5>.
- Roy, A. G., Siddiqui, S., Pölsterl, S., Navab, N., and Wachinger, C. Braintorrent: A peer-to-peer environment for decentralized federated learning. *arXiv preprint arXiv:1905.06731*, 2019.
- Sahu, A. K., Li, T., Sanjabi, M., Zaheer, M., Talwalkar, A., and Smith, V. On the convergence of federated optimization in heterogeneous networks. *arXiv preprint arXiv:1812.06127*, pp. 3, 2018.
- Simonyan, K. and Zisserman, A. Very deep convolutional networks for large-scale image recognition. *arXiv preprint arXiv:1409.1556*, 2014.
- Sun, T., Li, D., and Wang, B. Decentralized federated averaging. *IEEE Transactions on Pattern Analysis and Machine Intelligence*, 2022.
- Wang, H., Marella, S., and Anderson, J. Fedadmm: A federated primal-dual algorithm allowing partial participation. *arXiv preprint arXiv:2203.15104*, 2022.
- Wang, J., Charles, Z., Xu, Z., Joshi, G., McMahan, H. B., Al-Shedivat, M., Andrew, G., Avestimehr, S., Daly, K., Data, D., et al. A field guide to federated optimization. *arXiv preprint arXiv:2107.06917*, 2021.
- Xiao, H., Rasul, K., and Vollgraf, R. Fashion-mnist: a novel image dataset for benchmarking machine learning algorithms. *arXiv preprint arXiv:1708.07747*, 2017.
- Yang, H., Fang, M., and Liu, J. Achieving linear speedup with partial worker participation in non-IID federated learning. In *International Conference on Learning Representations*, 2021.
- Ye, H. and Zhang, T. Deepca: Decentralized exact pca with linear convergence rate. *J. Mach. Learn. Res.*, 22(238): 1–27, 2021.
- Ye, H., Zhou, Z., Luo, L., and Zhang, T. Decentralized accelerated proximal gradient descent. *Advances in Neural Information Processing Systems*, 33:18308–18317, 2020.
- Yu, H., Yang, S., and Zhu, S. Parallel restarted sgd with faster convergence and less communication: Demystifying why model averaging works for deep learning. In *Proceedings of the AAAI Conference on Artificial Intelligence*, pp. 5693–5700, 2019.
- Zhao, Y., Zhang, H., and Hu, X. Penalizing gradient norm for efficiently improving generalization in deep learning. In *International Conference on Machine Learning, ICML*, pp. 26982–26992. PMLR, 2022.

Supplementary Material for
 “Improving the Model Consistency of Decentralized Federated Learning”

A. Communication Network Topologies

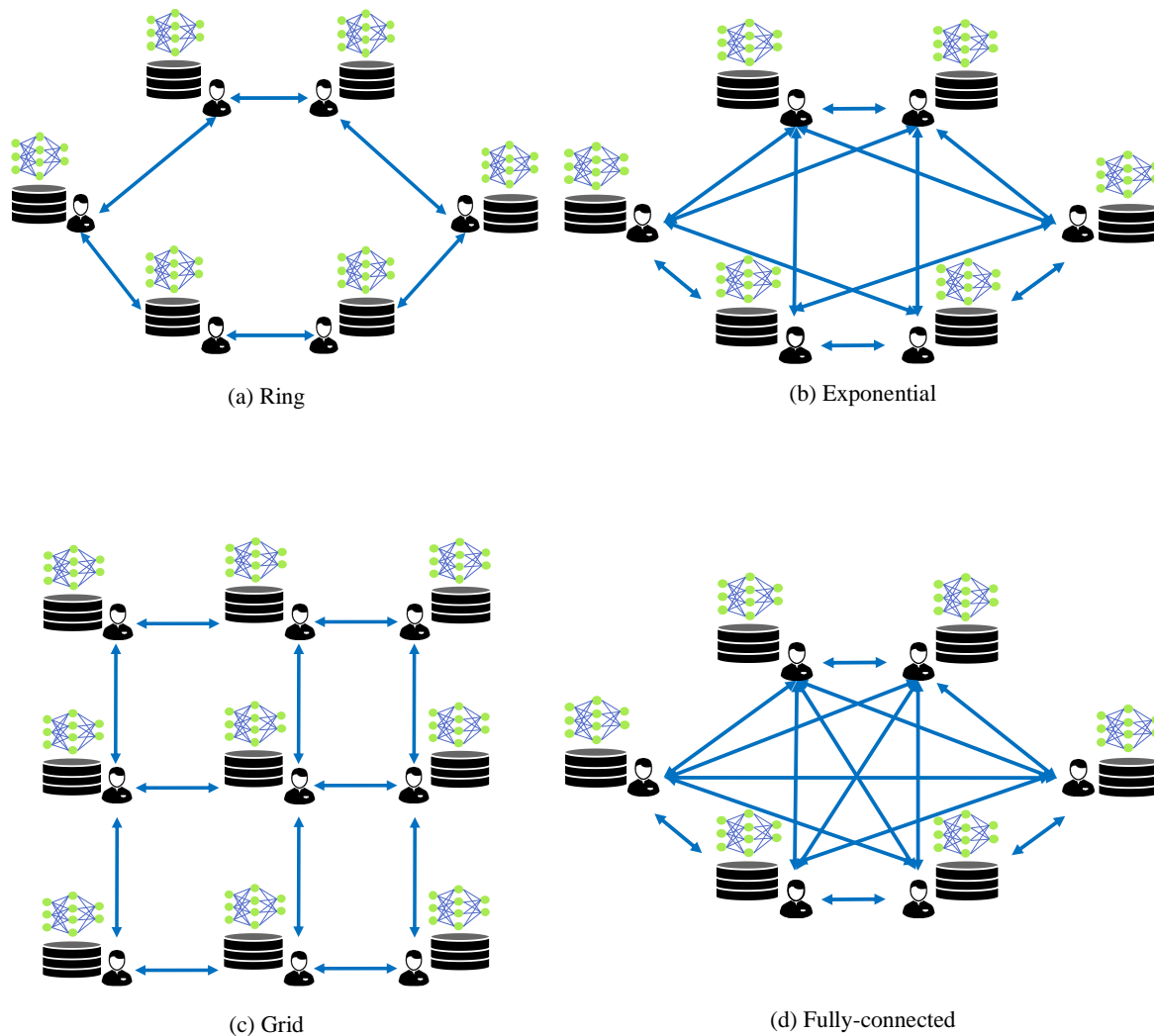


Figure 6. An overview of the various communication network topologies in decentralized setting.

B. More Details on Algorithm Implementation

B.1. Datasets and backbones.

CIFAR-10 and CIFAR-100 (Krizhevsky et al., 2009) are labeled subsets of the 80 million images dataset. They both share the same 60,000 input images. CIFAR-100 has a finer labeling, with 100 unique labels, in comparison to CIFAR-10, having 10 unique labels. The VGG-11 as the backbone is used for CIFAR-10, and the ResNet is chosen for CIFAR-100, where the batch-norm layers are replaced by group-norm layers due to a detrimental effect of batch-norm.

B.2. More details about baselines.

FedAvg is the classic FL method via the vanilla weighted averaging to parallel train a global model with a central server. FedSAM applies SAM to be the local optimizer for improving the model generalization performance. For decentralized schemes, D-PSGD is a classic decentralized parallel SGD method to reach a consensus model¹, DFedAvg is the decentralized FedAvg, and DFedAvgM uses SGD with momentum based on DFedAvg to train models on each client and performs multiple local training steps before each communication. Furthermore, DisPFL is a novel personalized FL framework in a decentralized communication protocol, which uses a decentralized sparse training technique, thus for a fair comparison, we report the global accuracy in DisPFL.

B.3. Hyperparameters.

The total client number is set to 100, and the number of connections in each client is restricted to at most 10 neighbors in the decentralized setting. For the centralized setting, the sample ratio of the client is set to 0.1. The local learning rate is set to 0.1 and decays with 0.998 after each communication round for all experiments, and the global learning rate is set to 1.0 for centralized methods. The batch size is fixed to 128 for all experiments. We run 1000 global communication rounds for CIFAR-10 and CIFAR-100. The SGD optimizer is used with a weighted decayed parameter 0.0005 for all baselines except FedSAM. Other optimizer hyper-parameters $\rho = 0.01$ for our algorithms (DFedSAM and DFedSAM-MGS with $Q = 1$) via grid search on the set $\{0.01, 0.025, 0.05, 0.1, 0.2, 0.4, 0.6, 0.8, 1.0\}$ and the value of ρ in FedSAM is followed by (Qu et al., 2022), respectively. And following by (Sun et al., 2022), the local optimization with momentum 0.9 for DFedAvgM. For local iterations K , the training epoch in D-PSGD is set to 1, that for all other methods is set to 5.

B.4. Communication configurations.

Specifically, such as (Dai et al., 2022), the decentralized methods actually generate far more communication volume than centralized methods because each client in the network topology needs to transmit the local information to their neighbors. However, only the partly sampled clients can upload their parameter updates with a central server in the centralized setting. Therefore, for a fair comparison, we use a dynamic time-varying connection topology for decentralized methods in Section 5.2, we restrict each client to communicate with at most 10 neighbors which are randomly sampled without replacement from all clients, and only 10 clients who are neighbors to each other can perform one gossip step to exchange their local information in DFedSAM. In DFedSAM-MGS, the gossip step is performed Q times, $10 \times Q$ clients are sampled without replacement to perform one gossip step to exchange their local information.

C. Preliminary Lemmas

Lemma C.1. [Lemma 4, (Lian et al., 2017)] For any $t \in \mathbb{Z}^+$, the mixing matrix $\mathbf{W} \in \mathbb{R}^m$ satisfies $\|\mathbf{W}^t - \mathbf{P}\|_{\text{op}} \leq \lambda^t$, where $\lambda := \max\{|\lambda_2|, |\lambda_m(W)|\}$ and for a matrix \mathbf{A} , we denote its spectral norm as $\|\mathbf{A}\|_{\text{op}}$. Furthermore, $\mathbf{1} := [1, 1, \dots, 1]^\top \in \mathbb{R}^m$ and

$$\mathbf{P} := \frac{\mathbf{1}\mathbf{1}^\top}{m} \in \mathbb{R}^{m \times m}.$$

In [Proposition 1, (Nedic & Ozdaglar, 2009)], the author also proved that $\|\mathbf{W}^t - \mathbf{P}\|_{\text{op}} \leq C\lambda^t$ for some $C > 0$ that depends on the matrix.

Lemma C.2. [Lemma A.5, (Qu et al., 2022)] (Bounded global variance of $\|\nabla f_i(\mathbf{x} + \delta_i) - \nabla f(\mathbf{x} + \delta)\|^2$.) An immediate implication of Assumptions 4.3 and 4.4, the variance of local and global gradients with perturbation can be bounded as follows:

$$\|\nabla f_i(\mathbf{x} + \delta_i) - \nabla f(\mathbf{x} + \delta)\|^2 \leq 3\sigma_g^2 + 6L^2\rho^2.$$

Lemma C.3. [Lemma B.1, (Qu et al., 2022)] (Bounded \mathcal{E}_δ of DFedSAM.) the updates of DFedSAM for any learning rate satisfying $\eta \leq \frac{1}{4KL}$ have the drift due to $\delta_{i,k} - \delta$:

$$\mathcal{E}_\delta = \frac{1}{m} \sum_{i=1}^m \mathbb{E}[\|\delta_{i,k} - \delta\|^2] \leq 2K^2\beta^2\eta^2\rho^2.$$

¹In this work, we focus on decentralized FL which refers to the local training with multiple local iterates, whereas decentralized learning/training focuses on one-step local training. For instance, D-PSGD (Lian et al., 2017) is a decentralized training algorithm, which uses the one-step SGD to train local models in each communication round.

where $\delta = \rho \frac{\nabla F(\mathbf{x})}{\|\nabla F(\mathbf{x})\|}$, $\delta_{i,k} = \rho \frac{\nabla F_i(\mathbf{y}^{t,k}, \xi)}{\|\nabla F_i(\mathbf{y}^{t,k}, \xi)\|}$.

D. Convergence Analysis for DFedSAM and DFedSAM-MGS

In the following, we present the proof of convergence results for DFedSAM and DFedSAM-MGS, respectively. Note that the proof of **Theorem 4.5** is thoroughly introduced in two sections **D.2** and **D.3** as follows, where $Q = 1$ and $Q > 1$, respectively.

D.1. Preliminary Lemmas

Lemma D.1. Assume that Assumptions 4.3 and 4.4 hold, and $(\mathbf{y}^{t,k}(i) + \delta_{i,k})_{t \geq 0}$, $(\mathbf{x}^{t,k}(i))_{t \geq 0}$ are generated by DFedSAM for all $i \in \{1, 2, \dots, m\}$. If the client update of DFedSAM for any learning rate $\eta \leq \frac{1}{10KL}$, it then follows:

$$\begin{aligned} \frac{1}{m} \sum_{i=1}^m \mathbb{E} \left\| (\mathbf{y}^{t,k}(i) + \delta_{i,k}) - \mathbf{x}^t(i) \right\|^2 &\leq 2K \left(\frac{4K^3 L^2 \eta^2 \rho^4}{2K-1} + 8K \eta^2 (L^2 \rho^2 + \sigma_g^2 + \sigma_l^2) \right) \\ &+ \frac{8K \eta^2}{m} \sum_{i=1}^m \mathbb{E} \left\| \nabla f(\mathbf{x}^t(i)) \right\|^2 + \frac{2K \rho^2}{2K-1}, \end{aligned} \quad (8)$$

where $0 \leq k \leq K-1$.

Proof.

For any local iteration $k \in \{0, 1, \dots, K-1\}$ in any node i , it holds

$$\begin{aligned} \frac{1}{m} \sum_{i=1}^m \mathbb{E} \left\| (\mathbf{y}^{t,k}(i) + \delta_{i,k}) - \mathbf{x}^t(i) \right\|^2 &= \frac{1}{m} \sum_{i=1}^m \mathbb{E} \left\| \mathbf{y}^{t,k-1}(i) + \delta_{i,k} - \eta \nabla F_i(\mathbf{y}^{t,k-1}(i) + \delta_{i,k-1}) - \mathbf{x}^t(i) \right\|^2 \\ &= \frac{1}{m} \sum_{i=1}^m \mathbb{E} \left\| \mathbf{y}^{t,k-1}(i) + \delta_{i,k-1} - \mathbf{x}^t(i) + \delta_{i,k} - \delta_{i,k-1} - \eta \left(\nabla F_i(\mathbf{y}^{t,k-1}(i) + \delta_{i,k-1}) - \nabla F_i(\mathbf{y}^{t,k-1}) \right) \right. \\ &\quad \left. + \nabla F_i(\mathbf{y}^{t,k-1}) - \nabla f_i(\mathbf{x}^t) + \nabla f_i(\mathbf{x}^t) - \nabla f(\mathbf{x}^t) + \nabla f(\mathbf{x}^t) \right\|^2 \\ &\leq \text{I} + \text{II}, \end{aligned}$$

where $\text{I} = (1 + \frac{1}{2K-1}) \frac{1}{m} \sum_{i=1}^m \left(\mathbb{E} \left\| \mathbf{y}^{t,k-1}(i) + \delta_{i,k-1} - \mathbf{x}^t(i) \right\|^2 + \mathbb{E} \|\delta_{i,k} - \delta_{i,k-1}\|^2 \right)$ and

$$\begin{aligned} \text{II} &= \frac{2K}{m} \sum_{i=1}^m \mathbb{E} \left\| -\eta \left(\nabla F_i(\mathbf{y}^{t,k-1}(i) + \delta_{i,k-1}) - \nabla F_i(\mathbf{y}^{t,k-1}) \right) \right. \\ &\quad \left. + \nabla F_i(\mathbf{y}^{t,k-1}) - \nabla f_i(\mathbf{x}^t) + \nabla f_i(\mathbf{x}^t) - \nabla f(\mathbf{x}^t) + \nabla f(\mathbf{x}^t) \right\|^2, \end{aligned}$$

With **Lemma C.3** and Assumptions, the bounds are

$$\text{I} = \left(1 + \frac{1}{2K-1}\right) \frac{1}{m} \sum_{i=1}^m \left(\mathbb{E} \left\| \mathbf{y}^{t,k-1}(i) + \delta_{i,k-1} - \mathbf{x}^t(i) \right\|^2 + 2K^2 L^2 \eta^2 \rho^4 \right),$$

and

$$\text{II} = \frac{8K \eta^2}{m} \sum_{i=1}^m \left(L^2 \rho^2 + \sigma_l^2 + \sigma_g^2 + \mathbb{E} \left\| \nabla f(\mathbf{x}^t) \right\|^2 \right),$$

where $\mathbb{E} \|\delta_{i,k-1}\|^2 \leq \rho^2$.

Thus, we can obtain

$$\begin{aligned} \mathbb{E} \left\| (\mathbf{y}^{t,k}(i) + \delta_{i,k}) - \mathbf{x}^t(i) \right\|^2 &\leq \left(1 + \frac{1}{2K-1}\right) \mathbb{E} \left\| (\mathbf{y}^{t,k-1}(i) + \delta_{i,k-1}) - \mathbf{x}^t(i) \right\|^2 \\ &\quad + \frac{4K^3 L^2 \eta^2 \rho^4}{2K-1} + 8K \eta^2 (L^2 \rho^2 + \sigma_g^2 + \sigma_l^2) + \frac{8K \eta^2}{m} \sum_{i=1}^m \mathbb{E} \left\| \nabla f(\mathbf{x}^t(i)) \right\|^2, \end{aligned}$$

where $\mathbb{E} \|\nabla f(\mathbf{x}^t)\|^2 = \frac{1}{m} \sum_{i=1}^m \mathbb{E} \|\nabla f(\mathbf{x}^t(i))\|^2$, $f(\mathbf{x}) := \frac{1}{m} \sum_{i=1}^m f_i(\mathbf{x})$, and $\nabla f_i(\mathbf{x}^t) := \nabla f(\mathbf{x}^t(i))$. The recursion from $\tau = 0$ to k yields

$$\begin{aligned} \frac{1}{m} \sum_{i=1}^m \mathbb{E} \|(\mathbf{y}^{t,k}(i) + \delta_{i,k}) - \mathbf{x}^t(i)\|^2 &\leq \frac{1}{m} \sum_{i=1}^m \sum_{\tau=1}^{K-1} \left(1 + \frac{1}{2K-1}\right)^\tau \left(\frac{4K^3 L^2 \eta^2 \rho^4}{2K-1} + 8K\eta^2(L^2 \rho^2 + \sigma_g^2 + \sigma_i^2)\right) \\ &\quad + \frac{8K\eta^2}{m} \sum_{i=1}^m \mathbb{E} \|\nabla f(\mathbf{x}^t(i))\|^2 + \left(1 + \frac{1}{2K-1}\right) \rho^2 \\ &\leq 2K \left(\frac{4K^3 L^2 \eta^2 \rho^4}{2K-1} + 8K\eta^2(L^2 \rho^2 + \sigma_g^2 + \sigma_i^2)\right) \\ &\quad + \frac{8K\eta^2}{m} \sum_{i=1}^m \mathbb{E} \|\nabla f(\mathbf{x}^t(i))\|^2 + \frac{2K\rho^2}{2K-1}. \end{aligned}$$

This completes the proof.

Lemma D.2. Assume that the number of local iterations K is large enough. Let $\{\mathbf{x}^t(i)\}_{t \geq 0}$ be generated by DFedSAM for all $i \in \{1, 2, \dots, m\}$ and any learning rate $\eta > 0$, we have following bound:

$$\frac{1}{m} \sum_{i=1}^m \mathbb{E} \|\mathbf{x}^{t,k}(i) - \bar{\mathbf{x}}^t\|^2 \leq \frac{C_2 \eta^2}{(1-\lambda)^2},$$

where $C_2 = 2K \left(\frac{4K^3 L^2 \rho^4}{2K-1} + 8K(L^2 \rho^2 + \sigma_g^2 + \sigma_i^2)\right) + \frac{8K}{m} \sum_{i=1}^m \mathbb{E} \|\nabla f(\mathbf{x}^t(i))\|^2 + \frac{2K\rho^2}{\eta^2(2K-1)}$.

Proof.

Following [Lemma 4, (Sun et al., 2022)], we denote $\mathbf{Z}^t := [\mathbf{z}^t(1), \mathbf{z}^t(2), \dots, \mathbf{z}^t(m)]^\top \in \mathbb{R}^{m \times d}$. With these notation, we have

$$\mathbf{X}^{t+1} = \mathbf{WZ}^t = \mathbf{WX}^t - \zeta^t, \quad (9)$$

where $\zeta^t := \mathbf{WX}^t - \mathbf{WZ}^t$. The iteration equation (9) can be rewritten as the following expression

$$\mathbf{X}^t = \mathbf{W}^t \mathbf{X}^0 - \sum_{j=0}^{t-1} \mathbf{W}^{t-1-j} \zeta^j. \quad (10)$$

Obviously, it follows

$$\mathbf{WP} = \mathbf{PW} = \mathbf{P}. \quad (11)$$

According to Lemma C.1, it holds

$$\|\mathbf{W}^t - \mathbf{P}\| \leq \lambda^t.$$

Multiplying both sides of equation (10) with \mathbf{P} and using equation (11), we then get

$$\mathbf{PX}^t = \mathbf{PX}^0 - \sum_{j=0}^{t-1} \mathbf{P}\zeta^j = - \sum_{j=0}^{t-1} \mathbf{P}\zeta^j, \quad (12)$$

where we used initialization $\mathbf{X}^0 = \mathbf{0}$. Then, we are led to

$$\begin{aligned} \|\mathbf{X}^t - \mathbf{PX}^t\| &= \left\| \sum_{j=0}^{t-1} (\mathbf{P} - \mathbf{W}^{t-1-j}) \zeta^j \right\| \\ &\leq \sum_{j=0}^{t-1} \|\mathbf{P} - \mathbf{W}^{t-1-j}\|_{op} \|\zeta^j\| \leq \sum_{j=0}^{t-1} \lambda^{t-1-j} \|\zeta^j\|. \end{aligned} \quad (13)$$

With Cauchy inequality,

$$\begin{aligned} \mathbb{E} \|\mathbf{X}^t - \mathbf{PX}^t\|^2 &\leq \mathbb{E} \left(\sum_{j=0}^{t-1} \lambda^{\frac{t-1-j}{2}} \cdot \lambda^{\frac{t-1-j}{2}} \|\zeta^j\| \right)^2 \\ &\leq \left(\sum_{j=0}^{t-1} \lambda^{t-1-j} \right) \left(\sum_{j=0}^{t-1} \lambda^{t-1-j} \mathbb{E} \|\zeta^j\|^2 \right) \end{aligned}$$

Direct calculation gives us

$$\mathbb{E}\|\zeta^j\|^2 \leq \|\mathbf{W}\|^2 \cdot \mathbb{E}\|\mathbf{X}^j - \mathbf{Z}^j\|^2 \leq \mathbb{E}\|\mathbf{X}^j - \mathbf{Z}^j\|^2.$$

With **Lemma D.1** and Assumption 3, for any j ,

$$\begin{aligned} & \mathbb{E}\|\mathbf{X}^j - \mathbf{Z}^j\|^2 \\ & \leq m \left(2K \left(\frac{4K^3 L^2 \rho^4}{2K-1} + 8K(L^2 \rho^2 + \sigma_g^2 + \sigma_l^2) + \frac{8K}{m} \sum_{i=1}^m \mathbb{E}\|\nabla f(\mathbf{x}^t(i))\|^2 \right) + \frac{2K\rho^2}{\eta^2(2K-1)} \right) \eta^2. \end{aligned}$$

Thus, we get

$$\begin{aligned} & \mathbb{E}\|\mathbf{X}^t - \mathbf{P}\mathbf{X}^t\|^2 \\ & \leq \frac{m \left(2K \left(\frac{4K^3 L^2 \rho^4}{2K-1} + 8K(L^2 \rho^2 + \sigma_g^2 + \sigma_l^2) + \frac{8K}{m} \sum_{i=1}^m \mathbb{E}\|\nabla f(\mathbf{x}^t(i))\|^2 \right) + \frac{2K\rho^2}{\eta^2(2K-1)} \right) \eta^2}{(1-\lambda)^2}. \end{aligned}$$

The fact that $\mathbf{X}^t - \mathbf{P}\mathbf{X}^t = \begin{pmatrix} \mathbf{x}^t(1) - \bar{\mathbf{x}}^t \\ \mathbf{x}^t(2) - \bar{\mathbf{x}}^t \\ \vdots \\ \mathbf{x}^t(m) - \bar{\mathbf{x}}^t \end{pmatrix}$ then proves the result.

Lemma D.3. Assume that the number of local iteration K is large enough. Let $\{\mathbf{x}^t(i)\}_{t \geq 0}$ be generated by DFedSAM-MGS for all $i \in \{1, 2, \dots, m\}$ and any learning rate $\eta > 0$, we have following bound:

$$\frac{1}{m} \sum_{i=1}^m \mathbb{E}\|\mathbf{x}^{t,k}(i) - \bar{\mathbf{x}}^t\|^2 \leq C_2 \eta^2 \left(\frac{\lambda^Q + 1}{(1-\lambda)^2 m^{2(Q-1)}} + \frac{\lambda^Q + 1}{(1-\lambda^Q)^2} \right),$$

where $C_2 = 2K \left(\frac{4K^3 L^2 \rho^4}{2K-1} + 8K(L^2 \rho^2 + \sigma_g^2 + \sigma_l^2) + \frac{8K}{m} \sum_{i=1}^m \mathbb{E}\|\nabla f(\mathbf{x}^t(i))\|^2 \right) + \frac{2K\rho^2}{\eta^2(2K-1)}$.

Proof.

Following [Lemma 4, (Sun et al., 2022)] and **Lemma D.2**, we denote $\mathbf{Z}^t := [\mathbf{z}^t(1), \mathbf{z}^t(2), \dots, \mathbf{z}^t(m)]^\top \in \mathbb{R}^{m \times d}$. With these notation, we have

$$\mathbf{X}^{t+1} = \mathbf{W}^Q \mathbf{Z}^t = \mathbf{W}^Q \mathbf{X}^t - \zeta^t, \quad (14)$$

where $\zeta^t := \mathbf{W}^Q \mathbf{X}^t - \mathbf{W}^Q \mathbf{Z}^t$. The iteration equation (14) can be rewritten as the following expression

$$\mathbf{X}^t = (\mathbf{W}^t)^Q \mathbf{X}^0 - \sum_{j=0}^{t-1} \mathbf{W}^{(t-1-j)Q} \zeta^j. \quad (15)$$

Obviously, it follows

$$\mathbf{W}^Q \mathbf{P} = \mathbf{P} \mathbf{W}^Q = \mathbf{P}. \quad (16)$$

According to Lemma C.1, it holds

$$\|\mathbf{W}^t - \mathbf{P}\| \leq \lambda^t.$$

Multiplying both sides of equation (15) with \mathbf{P} and using equation (16), we then get

$$\mathbf{P}\mathbf{X}^t = \mathbf{P}\mathbf{X}^0 - \sum_{j=0}^{t-1} \mathbf{P}\zeta^j = - \sum_{j=0}^{t-1} \mathbf{P}\zeta^j,$$

where we used initialization $\mathbf{X}^0 = \mathbf{0}$. Then, we are led to

$$\begin{aligned}
 \|\mathbf{X}^t - \mathbf{P}\mathbf{X}^t\| &= \left\| \sum_{j=0}^{t-1} (\mathbf{P} - \mathbf{W}^{Q(t-1-j)}) \zeta^j \right\| \\
 &\leq \sum_{j=0}^{t-1} \|\mathbf{P} - \mathbf{W}^{Q(t-1-j)}\|_{op} \|\zeta^j\| \\
 &\leq \sum_{j=0}^{t-1} \lambda^{t-1-j} \|\mathbf{W}^{(t-1-j)(Q-1)}\| \|\zeta^j\| \\
 &\leq \sum_{j=0}^{t-1} \lambda^{t-1-j} \|\mathbf{W}^{t-1-j} - \mathbf{P} + \mathbf{P}\|^{Q-1} \|\zeta^j\|.
 \end{aligned}$$

With Cauchy inequality,

$$\begin{aligned}
 \mathbb{E}\|\mathbf{X}^t - \mathbf{P}\mathbf{X}^t\|^2 &\leq \left(\sum_{j=0}^{t-1} \lambda^{t-1-j} (\lambda^{(Q-1)(t-1-j)} + \frac{1}{m^{Q-1}}) \sum_{j=0}^{t-1} \lambda^{t-1-j} (\lambda^{(Q-1)(t-1-j)} + \frac{1}{m^{Q-1}}) \mathbb{E}\|\zeta^j\|^2 \right) \\
 &\leq \left(\sum_{j=0}^{t-1} (\lambda^{Q(t-1-j)} + \frac{\lambda^{t-1-j}}{m^{Q-1}}) \sum_{j=0}^{t-1} (\lambda^{Q(t-1-j)} + \frac{\lambda^{t-1-j}}{m^{Q-1}}) \mathbb{E}\|\zeta^j\|^2 \right) \\
 &\leq \mathbb{E}\|\zeta^j\|^2 \left(\frac{1}{(1-\lambda)^2 m^{2(Q-1)}} + \frac{1}{(1-\lambda^Q)^2} \right).
 \end{aligned}$$

Direct calculation gives us

$$\begin{aligned}
 \mathbb{E}\|\zeta^j\|^2 &\leq \|\mathbf{W}^Q\|^2 \cdot \mathbb{E}\|\mathbf{X}^j - \mathbf{Z}^j\|^2 \\
 &\leq \|\mathbf{W} - \mathbf{P} + \mathbf{P}\|^{2Q} \mathbb{E}\|\mathbf{X}^j - \mathbf{Z}^j\|^2 \\
 &\leq (\|\mathbf{W} - \mathbf{P}\|^{2Q} + \|\mathbf{P}\|^{2Q}) \mathbb{E}\|\mathbf{X}^j - \mathbf{Z}^j\|^2 \\
 &\leq (\lambda^Q + 1) \mathbb{E}\|\mathbf{X}^j - \mathbf{Z}^j\|^2.
 \end{aligned}$$

With **Lemma D.1** and Assumption 3, for any j ,

$$\begin{aligned}
 &\mathbb{E}\|\mathbf{X}^j - \mathbf{Z}^j\|^2 \\
 &\leq m \left(2K \left(\frac{4K^3 L^2 \rho^4}{2K-1} + 8K(L^2 \rho^2 + \sigma_g^2 + \sigma_l^2) + \frac{8K}{m} \sum_{i=1}^m \mathbb{E} \|\nabla f(\mathbf{x}^t(i))\|^2 \right) + \frac{2K\rho^2}{\eta^2(2K-1)} \right) \eta^2.
 \end{aligned}$$

Thus, we get

$$\mathbb{E}\|\mathbf{X}^t - \mathbf{P}\mathbf{X}^t\|^2 \leq m C_2 \eta^2 \left(\frac{\lambda^Q + 1}{(1-\lambda)^2 m^{2(Q-1)}} + \frac{\lambda^Q + 1}{(1-\lambda^Q)^2} \right),$$

where $C_2 = 2K \left(\frac{4K^3 L^2 \rho^4}{2K-1} + 8K(L^2 \rho^2 + \sigma_g^2 + \sigma_l^2) + \frac{8K}{m} \sum_{i=1}^m \mathbb{E} \|\nabla f(\mathbf{x}^t(i))\|^2 \right) + \frac{2K\rho^2}{\eta^2(2K-1)}$.

The fact that $\mathbf{X}^t - \mathbf{P}\mathbf{X}^t = \begin{pmatrix} \mathbf{x}^t(1) - \bar{\mathbf{x}}^t \\ \mathbf{x}^t(2) - \bar{\mathbf{x}}^t \\ \vdots \\ \mathbf{x}^t(m) - \bar{\mathbf{x}}^t \end{pmatrix}$ then proves the result.

D.2. Proof of convergence results for DFedSAM.

Noting that $\mathbf{P}\mathbf{X}^{t+1} = \mathbf{P}\mathbf{W}\mathbf{Z}^t = \mathbf{P}\mathbf{Z}^t$, that is also

$$\overline{\mathbf{x}^{t+1}} = \bar{\mathbf{z}}^t,$$

where $\mathbf{X} := [\mathbf{x}(1), \mathbf{x}(2), \dots, \mathbf{x}(m)]^\top \in \mathbb{R}^{m \times d}$ and $\mathbf{Z} := [\mathbf{z}(1), \mathbf{z}(2), \dots, \mathbf{z}(m)]^\top \in \mathbb{R}^{m \times d}$. Thus we have

$$\overline{\mathbf{x}^{t+1}} - \overline{\mathbf{x}^t} = \overline{\mathbf{x}^{t+1}} - \overline{\mathbf{z}^t} + \overline{\mathbf{z}^t} - \overline{\mathbf{x}^t} = \overline{\mathbf{z}^t} - \overline{\mathbf{x}^t}, \quad (17)$$

where $\overline{\mathbf{z}^t} := \frac{\sum_{i=1}^m \mathbf{z}^t(i)}{m}$ and $\overline{\mathbf{x}^t} := \frac{\sum_{i=1}^m \mathbf{x}^t(i)}{m}$. In each node,

$$\begin{aligned} \overline{\mathbf{z}^t} - \overline{\mathbf{x}^t} &= \frac{\sum_{i=1}^m (\sum_{k=0}^{K-1} \mathbf{y}^{t,k+1}(i) - \mathbf{y}^{t,k}(i))}{m} \\ &= \frac{\sum_{i=1}^m \sum_{k=0}^{K-1} (-\eta \tilde{\mathbf{g}}^{t,k}(i))}{m} \\ &= \frac{\sum_{i=1}^m \sum_{k=0}^{K-1} (-\eta \nabla F_i(\mathbf{y}^{t,k} + \rho \nabla F_i(\mathbf{y}^{t,k}; \xi) / \|\nabla F_i(\mathbf{y}^{t,k}; \xi)\|_2); \xi)}{m}. \end{aligned} \quad (18)$$

The Lipschitz continuity of ∇f :

$$\mathbb{E}f(\overline{\mathbf{x}^{t+1}}) \leq \mathbb{E}f(\overline{\mathbf{x}^t}) + \mathbb{E}\langle \nabla f(\overline{\mathbf{x}^t}), \overline{\mathbf{z}^t} - \overline{\mathbf{x}^t} \rangle + \frac{L}{2} \mathbb{E}\|\overline{\mathbf{x}^{t+1}} - \overline{\mathbf{x}^t}\|^2, \quad (19)$$

where we used (17).

And (18) is used:

$$\begin{aligned} \mathbb{E}\langle K \nabla f(\overline{\mathbf{x}^t}), (\overline{\mathbf{z}^t} - \overline{\mathbf{x}^t})/K \rangle &= \mathbb{E}\langle K \nabla f(\overline{\mathbf{x}^t}), -\eta \nabla f(\overline{\mathbf{x}^t}) + \eta \nabla f(\overline{\mathbf{x}^t}) + (\overline{\mathbf{z}^t} - \overline{\mathbf{x}^t})/K \rangle \\ &= -\eta K \mathbb{E}\|\nabla f(\overline{\mathbf{x}^t})\|^2 + \mathbb{E}\langle K \nabla f(\overline{\mathbf{x}^t}), \eta \nabla f(\overline{\mathbf{x}^t}) + (\overline{\mathbf{z}^t} - \overline{\mathbf{x}^t})/K \rangle \\ &\stackrel{a)}{=} -\eta K \mathbb{E}\|\nabla f(\overline{\mathbf{x}^t})\|^2 + \mathbb{E}\langle K \nabla f(\overline{\mathbf{x}^t}), \frac{\eta}{mK} \sum_{i=1}^m \sum_{k=0}^{K-1} (\nabla F_i(\frac{1}{m} \sum_{i=1}^m \mathbf{x}^t(i)) - \nabla F_i(\mathbf{y}^{t,k} + \delta_{i,k}; \xi)) \rangle \\ &\stackrel{b)}{\leq} -\eta K \mathbb{E}\|\nabla f(\overline{\mathbf{x}^t})\|^2 + \eta \mathbb{E}\|\nabla f(\overline{\mathbf{x}^t})\| \cdot \mathbb{E}\left\| \frac{L}{m^2} \sum_{i=1}^m \sum_{i=1}^m \sum_{k=0}^{K-1} (\mathbf{x}^t(i) - \mathbf{y}^{t,k} - \delta_{i,k}) \right\| \\ &\stackrel{c)}{\leq} \frac{-\eta K}{2} \mathbb{E}\|\nabla f(\overline{\mathbf{x}^t})\|^2 + \frac{\eta L^2 K^2}{2K} \left(2K \left(\frac{4K^3 L^2 \eta^2 \rho^4}{2K-1} + 8K \eta^2 (L^2 \rho^2 + \sigma_g^2 + \sigma_l^2) \right) \right. \\ &\quad \left. + \frac{8K \eta^2}{m} \sum_{i=1}^m \mathbb{E}\|\nabla f(\mathbf{x}^t(i))\|^2 + \frac{2K \rho^2}{2K-1} \right), \end{aligned} \quad (20)$$

where a) uses $\nabla f_i = \mathbb{E} \nabla F_i$ and $\nabla f = \frac{1}{m} \sum_{i=1}^m \nabla f_i$, b) uses the Lipschitz continuity, and c) uses **Lemma D.1**. Meanwhile, we can get

$$\begin{aligned} \frac{L}{2} \mathbb{E}\|\overline{\mathbf{x}^{t+1}} - \overline{\mathbf{x}^t}\|^2 &= \frac{L}{2} \mathbb{E}\|\overline{\mathbf{z}^t} - \overline{\mathbf{x}^t}\|^2 \leq \frac{L}{2} \frac{1}{m} \sum_{i=1}^m \|\mathbf{y}^{t,K}(i) - \mathbf{x}^t(i)\|^2 \\ &\leq \frac{L}{2} \mathbb{E}\left\| \frac{-\eta \sum_{i=1}^m \sum_{k=0}^{K-1} \nabla F_i(\mathbf{y}^{t,k} + \delta_{i,k}; \xi)}{m} \right\|^2 \\ &\leq \frac{\eta^2 L}{2m} \sum_{i=1}^m \sum_{k=0}^{K-1} \mathbb{E}\|\nabla F_i(\mathbf{y}^{t,k} + \delta_{i,k}; \xi) - \nabla F_i(\mathbf{y}^{t,k}; \xi) + \nabla F_i(\mathbf{y}^{t,k}; \xi) \\ &\quad - \nabla f_i(\mathbf{x}^t) + \nabla f_i(\mathbf{x}^t)\|^2 \\ &\stackrel{a)}{\leq} \frac{3\eta^2 K L}{2} \left(L^2 \rho^2 + \sigma_l^2 + \frac{1}{m} \sum_{i=1}^m \mathbb{E}\|\nabla f(\mathbf{x}^t(i))\|^2 \right), \end{aligned} \quad (21)$$

where $a)$ uses **Assumptions 4.3** and **4.4**.

Thus, (19) can be represented as

$$\begin{aligned} \mathbb{E}f(\bar{\mathbf{x}}^{t+1}) &\leq \mathbb{E}f(\bar{\mathbf{x}}^t) - \frac{\eta K}{2} \mathbb{E} \left\| \nabla \mathbb{E}f(\bar{\mathbf{x}}^t) \right\|^2 + \frac{\eta L^2 K}{2} C_1 \\ &\quad + \frac{8\eta^3 K^2 L^2}{m} \sum_{i=1}^m \mathbb{E} \left\| \nabla f(\mathbf{x}^t(i)) \right\|^2 + \frac{3\eta^2 KL}{2} \left(L^2 \rho^2 + \sigma_i^2 + \frac{1}{m} \sum_{i=1}^m \mathbb{E} \left\| \nabla f(\mathbf{x}^t(i)) \right\|^2 \right), \end{aligned} \quad (22)$$

where $C_1 = 2K \left(\frac{4K^3 L^2 \eta^2 \rho^4}{2K-1} + 8K\eta^2(L^2 \rho^2 + \sigma_g^2 + \sigma_l^2) \right) + \frac{2K\rho^2}{2K-1}$.

Furthermore, with **Lemma D.2**, we can get

$$\begin{aligned} \frac{1}{m} \sum_{i=1}^m \mathbb{E} \left\| \nabla f(\mathbf{x}^t(i)) \right\|^2 &\leq 2L^2 \frac{\sum_{i=1}^m \left\| \mathbf{x}^t(i) - \bar{\mathbf{x}}^t \right\|^2}{m} + 2\mathbb{E} \left\| \nabla f(\bar{\mathbf{x}}^t) \right\|^2 \\ &\stackrel{a)}{\leq} 2L^2 \frac{C_2 \eta^2}{(1-\lambda)^2} + 2\mathbb{E} \left\| \nabla f(\bar{\mathbf{x}}^t) \right\|^2, \end{aligned} \quad (23)$$

where $a)$ uses **Lemma D.2** and $C_2 = 2K \left(\frac{4K^3 L^2 \rho^4}{2K-1} + 8K(L^2 \rho^2 + \sigma_g^2 + \sigma_l^2) \right) + \frac{8K}{m} \sum_{i=1}^m \mathbb{E} \left\| \nabla f(\mathbf{x}^t(i)) \right\|^2 + \frac{2K\rho^2}{\eta^2(2K-1)}$.

Therefore, we have

$$\frac{1}{m} \sum_{i=1}^m \mathbb{E} \left\| \nabla f(\mathbf{x}^t(i)) \right\|^2 \leq \frac{2L^2 C_3 \eta^2 + 2(1-\lambda)^2 \mathbb{E} \left\| \nabla f(\bar{\mathbf{x}}^t) \right\|^2}{(1-\lambda)^2 - 32L^2 \eta^2 K^2}, \quad (24)$$

where $C_3 = 2K \left(\frac{4K^3 L^2 \rho^4}{2K-1} + 8K(L^2 \rho^2 + \sigma_g^2 + \sigma_l^2) \right) + \frac{2K\rho^2}{\eta^2(2K-1)}$.

And then, (19) can be represented as

$$\begin{aligned} \mathbb{E}f(\bar{\mathbf{x}}^{t+1}) &\leq \mathbb{E}f(\bar{\mathbf{x}}^t) - \frac{\eta K}{2} \mathbb{E} \left\| \nabla f(\bar{\mathbf{x}}^t) \right\|^2 + \frac{\eta L^2 K C_1}{2} + 8\eta^3 K^2 L^2 \left(\frac{2L^2 C_3 \eta^2 + 2(1-\lambda)^2 \mathbb{E} \left\| \nabla f(\bar{\mathbf{x}}^t) \right\|^2}{(1-\lambda)^2 - 32L^2 \eta^2 K^2} \right) \\ &\quad + \frac{3\eta^2 KL}{2} \left(L^2 \rho^2 + \sigma_i^2 + \frac{1}{m} \sum_{i=1}^m \mathbb{E} \left\| \nabla f(\mathbf{x}^t(i)) \right\|^2 \right) \\ &\stackrel{a)}{\leq} \mathbb{E}f(\bar{\mathbf{x}}^t) + (16\eta^3 K^2 L^2 - \frac{\eta K}{2} + 3\eta^2 KL) \mathbb{E} \left\| \nabla f(\bar{\mathbf{x}}^t) \right\|^2 + \frac{3\eta^2 KL}{2} (L^2 \rho^2 + \sigma_i^2) \\ &\quad + \frac{\eta K L^2 C_1}{2} + \frac{16\eta^5 K^2 L^4 C_3 + 3\eta^4 K L^3 C_3}{(1-\lambda)^2}. \end{aligned} \quad (25)$$

Where $a)$ uses (24) and η is a very small value, summing the inequality (25) from $t = 1$ to T , and then we can get the proved result as below:

$$\min_{1 \leq t \leq T} \mathbb{E} \left\| \nabla f(\bar{\mathbf{x}}^t) \right\|^2 \leq \frac{2f(\bar{\mathbf{x}}^1) - 2f^*}{T(\eta K - 32\eta^3 K^2 L^2 - 6\eta^2 KL)} + \frac{\frac{\eta L^2 K C_1}{2} + \frac{\eta^4 K L^3 C_3 (16\eta KL + 3)}{(1-\lambda)^2} + \frac{3\eta^2 KL}{2} (L^2 \rho^2 + \sigma_i^2)}{\eta K - 32\eta^3 K^2 L^2 - 6\eta^2 KL}.$$

If we choose the learning rate $\eta = \mathcal{O}(1/L\sqrt{KT})$ and $\eta \leq \frac{1}{10KL}$, the number of communication round T is large enough, we have

$$\min_{1 \leq t \leq T} \mathbb{E} \left\| \nabla f(\bar{\mathbf{x}}^t) \right\|^2 = \mathcal{O} \left(\frac{(f(\bar{\mathbf{x}}^1) - f^*) + L^2 \rho^2 + \sigma_l^2}{\sqrt{KT}} + \frac{K(L^2 \rho^2 + \sigma_g^2 + \sigma_l^2)}{T} + \frac{K^{3/2} L^2 \rho^4}{T^{3/2} (1-\lambda)^2} + \frac{L^2 \rho^2 + \sigma_g^2 + \sigma_l^2}{K^{1/2} T^{3/2} (1-\lambda)^2} \right).$$

When perturbation amplitude ρ proportional to the learning rate, e.g., $\rho = \mathcal{O}(\frac{1}{\sqrt{T}})$, and then we have:

$$\min_{1 \leq t \leq T} \mathbb{E} \left\| \nabla f(\bar{\mathbf{x}}^t) \right\|^2 = \mathcal{O} \left(\frac{(f(\bar{\mathbf{x}}^1) - f^*) + \sigma_l^2}{\sqrt{KT}} + \frac{K(\sigma_g^2 + \sigma_l^2)}{T} + \frac{L^2}{K^{1/2} T^{3/2}} + \frac{\sigma_g^2 + \sigma_l^2}{K^{1/2} T^{3/2} (1-\lambda)^2} \right).$$

Under **Definition 4.2**, we can get

$$\min_{1 \leq t \leq T} \mathbb{E} \left\| \nabla f(\bar{\mathbf{x}}^t) \right\|^2 = \mathcal{O} \left(\frac{(f(\bar{\mathbf{x}}^1) - f^*) + \sigma_l^2}{\sqrt{KT}} + \frac{K(\beta^2 + \sigma_l^2)}{T} + \frac{L^2}{K^{1/2}T^{3/2}} + \frac{\beta^2 + \sigma_l^2}{K^{1/2}T^{3/2}(1-\lambda)^2} \right).$$

This completes the proof.

D.3. Proof of convergence results for DFedSAM-MGS

With multiple gossiping steps, \mathbf{x}^0 and \mathbf{z}^0 are represented as \mathbf{x} and \mathbf{z} , respectively. Meanwhile, $\mathbf{Z}^{t,Q} = \mathbf{Z}^{t,0} \cdot \mathbf{W}^Q = \mathbf{Z}^t \cdot \mathbf{W}^Q$. Noting that $\mathbf{P}\mathbf{X}^{t+1} = \mathbf{P}\mathbf{W}^Q\mathbf{Z}^t = \mathbf{P}\mathbf{Z}^t (Q > 1)$, that is also

$$\overline{\mathbf{x}^{t+1}} = \overline{\mathbf{z}^t},$$

where $\mathbf{X} := [\mathbf{x}(1), \mathbf{x}(2), \dots, \mathbf{x}(m)]^\top \in \mathbb{R}^{m \times d}$ and $\mathbf{Z} := [\mathbf{z}(1), \mathbf{z}(2), \dots, \mathbf{z}(m)]^\top \in \mathbb{R}^{m \times d}$. Thus we have

$$\overline{\mathbf{x}^{t+1}} - \overline{\mathbf{x}^t} = \overline{\mathbf{x}^{t+1}} - \overline{\mathbf{z}^t} + \overline{\mathbf{z}^t} - \overline{\mathbf{x}^t} = \overline{\mathbf{z}^t} - \overline{\mathbf{x}^t}, \quad (26)$$

where $\overline{\mathbf{z}^t} := \frac{\sum_{i=1}^m \mathbf{z}^t(i)}{m}$ and $\overline{\mathbf{x}^t} := \frac{\sum_{i=1}^m \mathbf{x}^t(i)}{m}$. In each node,

$$\begin{aligned} \overline{\mathbf{z}^t} - \overline{\mathbf{x}^t} &= \frac{\sum_{i=1}^m (\sum_{k=0}^{K-1} \mathbf{y}^{t,k+1}(i) - \mathbf{y}^{t,k}(i))}{m} \\ &= \frac{\sum_{i=1}^m \sum_{k=0}^{K-1} (-\eta \tilde{\mathbf{g}}^{t,k}(i))}{m} \\ &= \frac{\sum_{i=1}^m \sum_{k=0}^{K-1} (-\eta \nabla F_i(\mathbf{y}^{t,k} + \rho \nabla F_i(\mathbf{y}^{t,k}; \xi) / \|\nabla F_i(\mathbf{y}^{t,k}; \xi)\|_2); \xi)}{m}. \end{aligned} \quad (27)$$

The Lipschitz continuity of ∇f :

$$\mathbb{E} f(\overline{\mathbf{x}^{t+1}}) \leq \mathbb{E} f(\overline{\mathbf{x}^t}) + \mathbb{E} \langle \nabla f(\overline{\mathbf{x}^t}), \overline{\mathbf{z}^t} - \overline{\mathbf{x}^t} \rangle + \frac{L}{2} \mathbb{E} \|\overline{\mathbf{x}^{t+1}} - \overline{\mathbf{x}^t}\|^2, \quad (28)$$

where we used (26).

And (27) is used:

$$\begin{aligned} &\mathbb{E} \langle K \nabla f(\overline{\mathbf{x}^t}), (\overline{\mathbf{z}^t} - \overline{\mathbf{x}^t})/K \rangle = \mathbb{E} \langle K \nabla f(\overline{\mathbf{x}^t}), -\eta \nabla f(\overline{\mathbf{x}^t}) + \eta \nabla f(\overline{\mathbf{x}^t}) + (\overline{\mathbf{z}^t} - \overline{\mathbf{x}^t})/K \rangle \\ &= -\eta K \mathbb{E} \left\| \nabla f(\overline{\mathbf{x}^t}) \right\|^2 + \mathbb{E} \langle K \nabla f(\overline{\mathbf{x}^t}), \eta \nabla f(\overline{\mathbf{x}^t}) + (\overline{\mathbf{z}^t} - \overline{\mathbf{x}^t})/K \rangle \\ &\stackrel{a)}{=} -\eta K \mathbb{E} \left\| \nabla f(\overline{\mathbf{x}^t}) \right\|^2 + \mathbb{E} \langle K \nabla f(\overline{\mathbf{x}^t}), \frac{\eta}{mK} \sum_{i=1}^m \sum_{k=0}^{K-1} (\nabla F_i(\frac{1}{m} \sum_{i=1}^m \mathbf{x}^t(i)) - \nabla F_i(\mathbf{y}^{t,k} + \delta_{i,k}; \xi)) \rangle \\ &\stackrel{b)}{\leq} -\eta K \mathbb{E} \left\| \nabla f(\overline{\mathbf{x}^t}) \right\|^2 + \eta \mathbb{E} \left\| \nabla f(\overline{\mathbf{x}^t}) \right\| \cdot \mathbb{E} \left\| \frac{L}{m^2} \sum_{i=1}^m \sum_{i=1}^m \sum_{k=0}^{K-1} (\mathbf{x}^t(i) - \mathbf{y}^{t,k} - \delta_{i,k}) \right\| \\ &\stackrel{c)}{\leq} \frac{-\eta K}{2} \mathbb{E} \left\| \nabla f(\overline{\mathbf{x}^t}) \right\|^2 + \frac{\eta L^2 K^2}{2K} \left(2K \left(\frac{4K^3 L^2 \eta^2 \rho^4}{2K-1} + 8K \eta^2 (L^2 \rho^2 + \sigma_g^2 + \sigma_l^2) \right) \right. \\ &\quad \left. + \frac{8K \eta^2}{m} \sum_{i=1}^m \mathbb{E} \|\nabla f(\mathbf{x}^t(i))\|^2 + \frac{2K \rho^2}{2K-1} \right), \end{aligned} \quad (29)$$

where $a)$ uses $\nabla f_i = \mathbb{E}\nabla F_i$ and $\nabla f = \frac{1}{m} \sum_{i=1}^m \nabla f_i$, $b)$ uses the Lipschitz continuity, and $c)$ uses **Lemma D.1**. Meanwhile, we can get

$$\begin{aligned}
 \frac{L}{2} \mathbb{E} \left\| \overline{\mathbf{x}^{t+1}} - \overline{\mathbf{x}^t} \right\|^2 &= \frac{L}{2} \mathbb{E} \left\| \overline{\mathbf{z}^t} - \overline{\mathbf{x}^t} \right\|^2 \leq \frac{L}{2} \frac{1}{m} \sum_{i=1}^m \left\| \mathbf{y}^{t,K}(i) - \mathbf{x}^t(i) \right\|^2 \\
 &\leq \frac{L}{2} \mathbb{E} \left\| \frac{-\eta \sum_{i=1}^m \sum_{k=0}^{K-1} \nabla F_i(\mathbf{y}^{t,k} + \delta_{i,k}; \xi)}{m} \right\|^2 \\
 &\leq \frac{\eta^2 L}{2m} \sum_{i=1}^m \sum_{k=0}^{K-1} \mathbb{E} \left\| \nabla F_i(\mathbf{y}^{t,k} + \delta_{i,k}; \xi) - \nabla F_i(\mathbf{y}^{t,k}; \xi) + \nabla F_i(\mathbf{y}^{t,k}; \xi) \right. \\
 &\quad \left. - \nabla f_i(\mathbf{x}^t) + \nabla f_i(\mathbf{x}^t) \right\|^2 \\
 &\stackrel{a)}{\leq} \frac{3\eta^2 KL}{2} \left(L^2 \rho^2 + \sigma_l^2 + \frac{1}{m} \sum_{i=1}^m \mathbb{E} \left\| \nabla f(\mathbf{x}^t(i)) \right\|^2 \right),
 \end{aligned} \tag{30}$$

where $a)$ uses **Assumptions 4.3** and **4.4**.

Thus, (28) can be represented as

$$\begin{aligned}
 \mathbb{E}f(\overline{\mathbf{x}^{t+1}}) &\leq \mathbb{E}f(\overline{\mathbf{x}^t}) - \frac{\eta K}{2} \mathbb{E} \left\| \nabla \mathbb{E}f(\overline{\mathbf{x}^t}) \right\|^2 + \frac{\eta L^2 K}{2} C_1 \\
 &\quad + \frac{8\eta^3 K^2 L^2}{m} \sum_{i=1}^m \mathbb{E} \left\| \nabla f(\mathbf{x}^t(i)) \right\|^2 + \frac{3\eta^2 KL}{2} \left(L^2 \rho^2 + \sigma_l^2 + \frac{1}{m} \sum_{i=1}^m \mathbb{E} \left\| \nabla f(\mathbf{x}^t(i)) \right\|^2 \right),
 \end{aligned} \tag{31}$$

where $C_1 = 2K \left(\frac{4K^3 L^2 \eta^2 \rho^4}{2K-1} + 8K\eta^2(L^2 \rho^2 + \sigma_g^2 + \sigma_l^2) + \frac{2K\rho^2}{2K-1} \right)$.

Furthermore, with **Lemma D.3**, we can get

$$\begin{aligned}
 \frac{1}{m} \sum_{i=1}^m \mathbb{E} \left\| \nabla f(\mathbf{x}^t(i)) \right\|^2 &\leq 2L^2 \frac{\sum_{i=1}^m \left\| \mathbf{x}^t(i) - \overline{\mathbf{x}^t} \right\|^2}{m} + 2\mathbb{E} \left\| \nabla f(\overline{\mathbf{x}^t}) \right\|^2 \\
 &\stackrel{a)}{\leq} 2L^2 C_2 \eta^2 \left(\frac{\lambda^Q + 1}{(1-\lambda)^2 m^{2(Q-1)}} + \frac{\lambda^Q + 1}{(1-\lambda^Q)^2} \right) + 2\mathbb{E} \left\| \nabla f(\overline{\mathbf{x}^t}) \right\|^2,
 \end{aligned} \tag{32}$$

where $a)$ uses **Lemma D.3** and $C_2 = 2K \left(\frac{4K^3 L^2 \rho^4}{2K-1} + 8K(L^2 \rho^2 + \sigma_g^2 + \sigma_l^2) + \frac{8K}{m} \sum_{i=1}^m \mathbb{E} \left\| \nabla f(\mathbf{x}^t(i)) \right\|^2 \right) + \frac{2K\rho^2}{\eta^2(2K-1)}$.

Moreover, we have

$$\frac{1}{m} \sum_{i=1}^m \mathbb{E} \left\| \nabla f(\mathbf{x}^t(i)) \right\|^2 \leq \frac{2L^2 C_3 \eta^2 \left(\frac{\lambda^Q + 1}{(1-\lambda)^2 m^{2(Q-1)}} + \frac{\lambda^Q + 1}{(1-\lambda^Q)^2} \right) + 2\mathbb{E} \left\| \nabla f(\overline{\mathbf{x}^t}) \right\|^2}{1 - 32L^2 \eta^2 K^2 \left(\frac{\lambda^Q + 1}{(1-\lambda)^2 m^{2(Q-1)}} + \frac{\lambda^Q + 1}{(1-\lambda^Q)^2} \right)}, \tag{33}$$

where $C_3 = 2K \left(\frac{4K^3 L^2 \rho^4}{2K-1} + 8K(L^2 \rho^2 + \sigma_g^2 + \sigma_l^2) + \frac{2K\rho^2}{\eta^2(2K-1)} \right)$.

Therefore, (28) is

$$\begin{aligned}
 \mathbb{E}f(\overline{\mathbf{x}^{t+1}}) &\leq \mathbb{E}f(\overline{\mathbf{x}^t}) - \frac{\eta K}{2} \mathbb{E} \left\| \nabla f(\overline{\mathbf{x}^t}) \right\|^2 + \frac{\eta L^2 K C_1}{2} + 8\eta^3 K^2 L^2 (2L^2 C_3 \eta^2 \left(\frac{\lambda^Q + 1}{(1-\lambda)^2 m^{2(Q-1)}} \right. \\
 &\quad \left. + \frac{\lambda^Q + 1}{(1-\lambda^Q)^2} \right) + 2\mathbb{E} \left\| \nabla f(\overline{\mathbf{x}^t}) \right\|^2) + \frac{3\eta^2 KL}{2} \left(L^2 \rho^2 + \sigma_l^2 + \frac{1}{m} \sum_{i=1}^m \mathbb{E} \left\| \nabla f(\mathbf{x}^t(i)) \right\|^2 \right) \\
 &\stackrel{a)}{\leq} \mathbb{E}f(\overline{\mathbf{x}^t}) + (16\eta^3 K^2 L^2 - \frac{\eta K}{2} + 3\eta^2 KL) \mathbb{E} \left\| \nabla f(\overline{\mathbf{x}^t}) \right\|^2 + \frac{3\eta^2 KL}{2} (L^2 \rho^2 + \sigma_l^2) \\
 &\quad + \frac{\eta K L^2 C_1}{2} + (16\eta^5 K^2 L^4 C_3 + 3\eta^4 K L^3 C_3) \left(\frac{\lambda^Q + 1}{(1-\lambda)^2 m^{2(Q-1)}} + \frac{\lambda^Q + 1}{(1-\lambda^Q)^2} \right).
 \end{aligned} \tag{34}$$

Where a) uses (33) and η is a very small value, summing the inequality (34) from $t = 1$ to T , and then we can get the proved result as below:

$$\begin{aligned} \min_{1 \leq t \leq T} \mathbb{E} \left\| \nabla f(\bar{\mathbf{x}}^t) \right\|^2 &\leq \frac{2f(\bar{\mathbf{x}}^1) - 2f^*}{T(\eta K - 32\eta^3 K^2 L^2 - 6\eta^2 K L)} \\ &+ \frac{\frac{\eta L^2 K C_1}{2} + \eta^4 K L^3 C_3 (16\eta K L + 3) \left(\frac{\lambda^Q + 1}{(1-\lambda)^2 m^{2(Q-1)}} + \frac{\lambda^Q + 1}{(1-\lambda^Q)^2} \right) + \frac{3\eta^2 K L}{2} (L^2 \rho^2 + \sigma_l^2)}{\eta K - 32\eta^3 K^2 L^2 - 6\eta^2 K L}. \end{aligned}$$

Summing the inequality (34) from $t = 1$ to T , and then we can get the proved result as below:

$$\min_{1 \leq t \leq T} \mathbb{E} \left\| \nabla f(\bar{\mathbf{x}}^t) \right\|^2 \leq \frac{2f(\bar{\mathbf{x}}^1) - 2f^*}{T(\eta K - 32\eta^3 K^2 L^2)} + \frac{\frac{\eta L^2 K C_1}{2} + 16C_2 \eta^5 K^2 L^4 \left(\frac{\lambda^Q + 1}{(1-\lambda)^2 m^{2(Q-1)}} + \frac{\lambda^Q + 1}{(1-\lambda^Q)^2} \right)}{\eta K - 32\eta^3 K^2 L^2}.$$

If we choose the learning rate $\eta = \mathcal{O}(1/L\sqrt{KT})$ and $\eta \leq \frac{1}{10KL}$, the number of communication round T is large enough with **Definition 4.2** and $\Phi(\lambda, m, Q) = \frac{\lambda^Q + 1}{(1-\lambda)^2 m^{2(Q-1)}} + \frac{\lambda^Q + 1}{(1-\lambda^Q)^2}$ is the key parameter to the convergence bound with the number of spectral gap, the clients and multiple gossiping steps. Thus we have

$$\min_{1 \leq t \leq T} \mathbb{E} \left\| \nabla f(\bar{\mathbf{x}}^t) \right\|^2 = \mathcal{O} \left(\frac{(f(\bar{\mathbf{x}}^1) - f^*) + L^2 \rho^2 + \sigma_l^2}{\sqrt{KT}} + \frac{K(L^2 \rho^2 + \sigma_g^2 + \sigma_l^2)}{T} + \Phi(\lambda, m, Q) \frac{K^2 L^2 \rho^4 + L^2 \rho^2 + \sigma_g^2 + \sigma_l^2}{K^{1/2} T^{3/2}} \right).$$

When perturbation amplitude ρ proportional to the learning rate, e.g., $\rho = \mathcal{O}(\frac{1}{\sqrt{T}})$, and then we have:

$$\min_{1 \leq t \leq T} \mathbb{E} \left\| \nabla f(\bar{\mathbf{x}}^t) \right\|^2 = \mathcal{O} \left(\frac{(f(\bar{\mathbf{x}}^1) - f^*) + \sigma_l^2}{\sqrt{KT}} + \frac{K(\beta^2 + \sigma_l^2)}{T} + \frac{L^2}{K^{1/2} T^{3/2}} + \Phi(\lambda, m, Q) \frac{\beta^2 + \sigma_l^2}{K^{1/2} T^{3/2}} \right).$$

This completes the proof.